

Article

A 3D Cuboid Image Encryption Algorithm Based on Controlled Alternate Quantum Walk of Message Coding

Pai Liu ¹, Shihua Zhou ^{1,*} and Wei Qi Yan ² 

¹ Key Laboratory of Advanced Design and Intelligent Computing, Ministry of Education, School of Software Engineering, Dalian University, Dalian 116622, China

² School of Engineering, Computer and Mathematical Sciences, Auckland University of Technology, Auckland 1010, New Zealand

* Correspondence: zhoushihua@dlu.edu.cn

Abstract: In order to solve various security risks faced by image privacy protection, we propose a 3D cuboid image encryption scheme based on message-encoded controlled alternate quantum walks. Firstly, we calculated the initial parameters of the quantum system and performed a one-dimensional quantum walk to generate a probability distribution sequence. Secondly, we encoded the sequence into a quaternary message using multiple sets of encoded messages to control the alternate quantum walk model, generating a 3D probability amplitude matrix and 3D probability distribution matrix to obtain the 3D quantum hash sequence through the 3D probability distribution matrix. Then, the image was divided into blocks and integrated into a cuboid. The image cuboid was scrambled between layers using the probability value sequence, and the 3D probability distribution matrix was used to complete the scrambling of the cross-section between layers. Finally, we converted each pixel value of the scrambled cuboid into a binary cube and controlled it to perform the rotation operation through the 3D probability magnitude matrix, then used the 3D quantum hash sequence to XOR the obtained cuboid image and tilted it to obtain the final encrypted image. The simulation results show that the image encryption scheme can resist various typical attacks and has good security performance.



Citation: Liu, P.; Zhou, S.; Yan, W.Q.

A 3D Cuboid Image Encryption Algorithm Based on Controlled Alternate Quantum Walk of Message Coding. *Mathematics* **2022**, *10*, 4441.
<https://doi.org/10.3390/math10234441>

Academic Editor: Daniel-Ioan Curiac

Received: 17 October 2022

Accepted: 22 November 2022

Published: 24 November 2022

Publisher's Note: MDPI stays neutral with regard to jurisdictional claims in published maps and institutional affiliations.



Copyright: © 2022 by the authors. Licensee MDPI, Basel, Switzerland. This article is an open access article distributed under the terms and conditions of the Creative Commons Attribution (CC BY) license (<https://creativecommons.org/licenses/by/4.0/>).

1. Introduction

With the development and rise of 5G, more and more devices are connected to a mobile network, and the data traffic on mobile networks has increased dramatically. In daily life, people process and transmit digital information on mobile networks through various devices every day, among which, digital image information accounts for a large proportion. Preventing digital images from being stolen and tampered with by attackers and ensuring information security is a research topic that cannot be ignored.

People can intuitively obtain a lot of information through images. To prevent image information from being attacked and tampered with, digital watermarking and image encryption technologies can be used to secure data [1–4]. It is necessary to encrypt images according to their characteristics that are different from text: reduce the amount of data contained in images, break the strong correlation between adjacent pixels, and reduce information redundancy [5,6]. Based on this idea, combined with chaos, DNA coding, and other theories, many researchers have proposed a variety of image encryption algorithms [7–16]. Mansouri et al. [17] proposed a one-dimensional chaotic mapping amplifier (1-DCMA) and used its generated chaotic sequence to design an asymmetric image encryption scheme which uses a key to add rows and implements a new index representation (IR) concept

using a shift sequence to manipulate the position and value of pixels synchronously. Cao et al. [3] proposed a 2D infinite collapse map and compared it with the existing 2D chaotic maps. Two-dimensional ICM has better ergodicity, hyper chaos, unpredictability, and a wider chaotic region. The image is encrypted by 2D-ICM, which makes the system more secure. Wang et al. [18] used the chaotic sequences generated by the Chen hyperchaotic system for interblock index scrambling and intrablock Fisher–Yates scrambling, and then diffused by different DNA encoding rules and different operating rules corresponding to the chaotic sequences, thereby improving the algorithm security. Encryption methods based on chaotic mapping have better performance. However, one-dimensional chaos-based ones only have a very limited range of parameters. Although hyperchaotic ones have a wider range of chaotic regions, most suffer from high-computational cost. In addition, researchers have proposed new methods for image encryption models based on fractal theory [19–21], optical theory [22,23], neural network models [4,24–27], compressed sensing [28,29], optimization algorithms [30–32], and quantum theory [33,34].

Quantum walks are divided into two models: continuous and discrete. Discrete quantum walks are nonlinear mappings between quantum operators and the probability of their occurrence positions and are extremely sensitive to the initial state. A discrete quantum walk ensures the security performance of the system through the infinite possibility of the initial state. It has similar characteristics to the chaotic dynamics in determining the walk state in the system, so it is used by researchers in image encryption models [35–37]. Yang et al. [38] used the nonlinear chaotic dynamic performance of a quantum walk (QW) to construct a key generator with good performance, and based on this, they proposed an image encryption algorithm that combines quantum computing with image encryption, which has better security. In addition, Yang et al. [39] designed a quantum hash function based on one-dimensional controlled alternating quantum walks and applied it to image encryption. Abd EL-Latif et al. [40] designed an image encryption mechanism based on the controlled alternating quantum walk model. The replacement and scrambling stages are based on independently calculated quantum walks, which well protect the patient privacy in the medical system. However, the initial parameters of the quantum wander described above are fixed, and the quantum wander key is fixed for different images, which has low security and poor key sensitivity. When performing a controlled alternating quantum wander, its controlled coin operator is relatively single, and the redundancy of binary messages is high. At the same time, it only encrypts the original image in the two-dimensional plane using the probability matrix, which has a limited effect on image dislocation and diffusion.

Based on the above research questions, in this paper, we propose a new 3D cuboid image encryption algorithm based on message-encoded controlled alternating quantum walks. In order to solve the problem of fixed initial parameters of quantum wandering, we designed a key set with good security that can calculate the initial parameters of the quantum system and perform a one-dimensional quantum walk to generate a probability distribution sequence. In order to avoid excessive message redundancy, we encoded this sequence into a quaternary message and used multiple sets of encoded messages to control the alternate quantum walk model. Meanwhile, we divided the plane image into blocks and converted it into a three-dimensional cuboid image for processing. Combined with the quantum mechanical properties of the quantum walk model, our scheme has good security performance and can effectively prevent digital image information from being stolen and tampered with by attackers.

The rest of this paper is organized as follows: Section 2 presents one-dimensional discrete quantum walks and controlled alternating quantum walks on circles. Section 3 presents 3D cuboid image encryption based on the message-encoded controlled alternating quantum walks model. The fourth section introduces the security performance analysis and testing of this model. The last section is the conclusion.

2. Preliminary Works

The quantum walk model is a quantization of the classical random walk model by using a quantized description of the position of the particle to construct the entanglement between the particle position and the quantized Markov state variable [35]. There are two models of quantum walks: discrete QWs and continuous QWs. Discrete quantum walks determine the motion state of the system and have similar properties to chaotic dynamics, which can be used in the process of image encryption algorithms. The discrete QWs model consists of two parts: the coin and the walker. The coin and the walker are in a Hilbert space $H_t = H_s \otimes H_o$. By applying a conditional shift operator to the coin operator, the moving state of the walker is changed. On an odd circle with T nodes, the probabilities at all points are essentially nonzero when $t \geq T - 1$.

2.1. One-Dimensional Discrete Quantum Walks (1DQWs) on Circles

A one-dimensional discrete quantum walk on a circle [38] whose initial state of the coin operator O is $|o\rangle = \alpha|0\rangle + \beta|1\rangle$, where α and β are the amplitudes of the initial coin operator which satisfy the normalization equation $|\alpha|^2 + |\beta|^2 = 1$. During the evolution of the quantum system, the quantum walk is realized by applying the shift operator to the coin operator, which is represented by the global unitary operator \hat{M} , such as in Equation (1):

$$\hat{M} = \hat{N}(\hat{I} \otimes \hat{O}) \quad (1)$$

where \hat{N} represents the shift operator, and its expression is Equation (2):

$$\hat{N} = \sum_x (|(x+1) \text{mod } T, 0\rangle\langle x, 0| + |(x-1) \text{mod } T, 1\rangle\langle x, 1|) \quad (2)$$

\hat{I} represents the identity matrix. \hat{O} represents the coin operator, and its expression is Equation (3):

$$\hat{O} = \begin{pmatrix} \cos \theta & \sin \theta \\ \sin \theta & -\cos \theta \end{pmatrix} \quad (3)$$

where $\theta \in [0, \frac{\pi}{2}]$.

After t steps, the final state of the entire quantum system is Equation (4):

$$|\psi\rangle_t = (\hat{M})^t |\psi\rangle_0 \quad (4)$$

After t steps, the probability of finding a walker at position x is Equation (5):

$$P(x, t) = \sum_{c \in \{0,1\}} |\langle x, c | (\hat{M})^t | \psi \rangle_0|^2 \quad (5)$$

The general situation of the probability distribution of one-dimensional discrete quantum walks on a circle (number of nodes 75; $\theta_0 = \frac{\pi}{3}$; step count $k = 165$; the initial coin operator is $c = \frac{1}{\sqrt{2}} \begin{bmatrix} 1 \\ 1 \end{bmatrix}$) is shown in Figure 1.

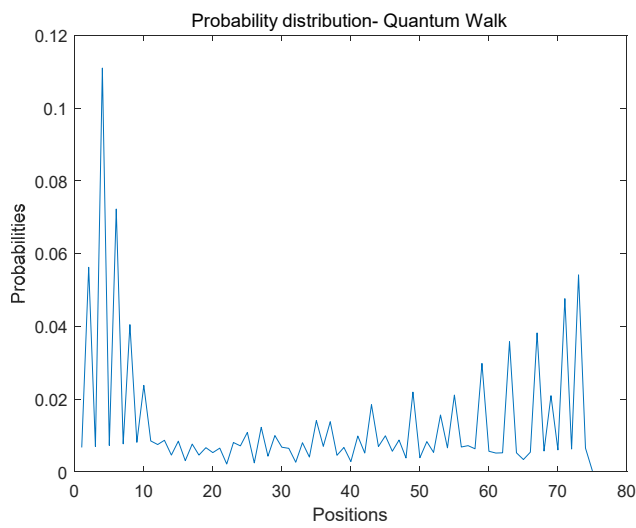


Figure 1. 1D discrete quantum walk probability distribution on a circle.

2.2. Controlled Alternate Quantum Walks (CAQWs) on Circles

A controlled alternate quantum walk process on a circle has a string of messages controlling the transform operator at each step [41]. When the t -th bit of the message is zero or one, the evolution operator \hat{M}_0 or \hat{M}_1 is applied to the coin operator, which is expressed as Equations (6) and (7):

$$\hat{M}_0 = \hat{N}_y(\hat{I} \otimes \hat{O}_0)\hat{N}_x(\hat{I} \otimes \hat{O}_0) \quad (6)$$

$$\hat{M}_1 = \hat{N}_y(\hat{I} \otimes \hat{O}_1)\hat{N}_x(\hat{I} \otimes \hat{O}_1) \quad (7)$$

where \hat{N}_x , \hat{N}_y represent the shift operators acting in the x and y directions, respectively, which are expressed as Equations (8) and (9):

$$\hat{N}_x = \sum_{x,y}^T (|(x+1) \bmod T, y, 0\rangle\langle x, y, 0| + |(x-1) \bmod T, y, 1\rangle\langle x, y, 1|) \quad (8)$$

$$\hat{N}_y = \sum_{x,y}^T (|x, (y+1) \bmod T, 0\rangle\langle x, y, 0| + |x, (y-1) \bmod T, 1\rangle\langle x, y, 1|) \quad (9)$$

\hat{I} represents the identity matrix. \hat{O}_0 , \hat{O}_1 represent two alternating coin operators, whose construction is in the following Equations (10) and (11):

$$\hat{O}_0 = \begin{pmatrix} \cos \theta_0 & \sin \theta_0 \\ \sin \theta_0 & -\cos \theta_0 \end{pmatrix} \quad (10)$$

$$\hat{O}_1 = \begin{pmatrix} \cos \theta_1 & \sin \theta_1 \\ \sin \theta_1 & -\cos \theta_1 \end{pmatrix} \quad (11)$$

After t steps, the final state of the entire quantum system is Equation (12):

$$|\psi\rangle_t = (\hat{M})^t |\psi\rangle_0 \quad (12)$$

After t steps, the magnitude of the probability of finding a walker at position (x, y) is Equation (13). The probability is Equation (14):

$$F(x, y, t) = \sum_{c \in \{0,1\}} \langle x, y, c | (\hat{M})^t | \psi \rangle_0 \quad (13)$$

$$P(x, y, t) = \sum_{c \in \{0,1\}} |\langle x, y, c | (\hat{M})^t | \psi \rangle_0|^2 \quad (14)$$

The probability distribution of quantum walks controlled by binary message string M on a circle (number of nodes: 19; $\theta_0 = \frac{\pi}{3}$; $\theta_1 = \frac{\pi}{5}$; the initial coin operator is $c = \frac{1}{\sqrt{2}} \begin{bmatrix} 1 \\ 1 \end{bmatrix}$; message = [010000001111010101010100101000000111101010101001]), as is shown in Figure 2.

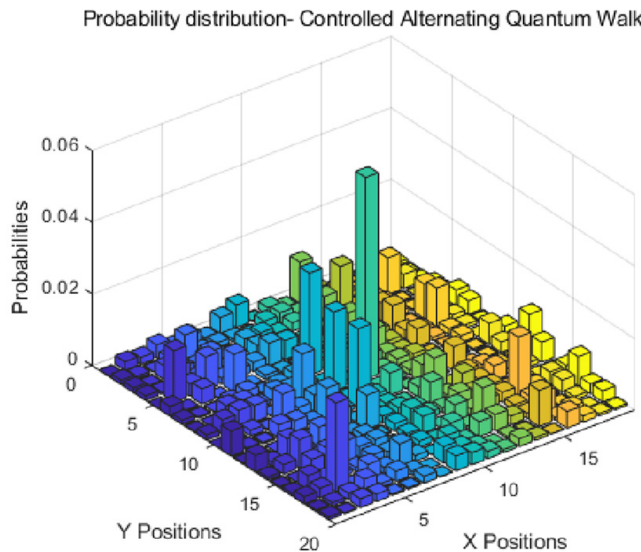


Figure 2. Controlled alternate quantum walk probability distribution on a circle.

3. Proposed Method

In the following subsections, we describe our proposed encryption algorithm in detail.

3.1. Generate Initial Key

Our key consists of four parts: initial parameters $d_1 \sim d_8$, $sumP$ of plaintext image pixel values, image block size $Bsize$, supplementary parameters $M1, N1$, and the number of blocks $Bnum$.

3.1.1. Initial Parameters $d_1 \sim d_8$

We took a plaintext image as the input of SHA-512 and obtained a 128-bit hexadecimal sequence which was divided into 64 groups of sequences $k_1 \sim k_{64}$. Each group was an 8-bit byte sequence. According to the 64 groups of sequences, we calculated and generated initial parameters $d_1 \sim d_8$ and use them as keys, such as in Equation (15), the specific steps are as follows:

Step one: Convert $k_1 \sim k_{32}$ to binary sequence.

Step two: Convert $k_{33} \sim k_{64}$ into a decimal sequence and take the entire sequence modulo 8 to obtain the cyclic shift bits of the sequence $k_1 \sim k_{32}$.

Step three: According to $k_{33} \sim k_{64}$, we need to rotate $k_1 \sim k_{32}$, convert it into a decimal sequence, and calculate the initial parameters $d_1 \sim d_8$.

$$\left\{ \begin{array}{l} d_1 = \frac{k_1 \ll mod(k_{33}, 8) + k_2 \ll mod(k_{34}, 8) + k_3 \ll mod(k_{35}, 8) + k_4 \ll mod(k_{36}, 8)}{4 * 256 + 1} \\ d_2 = \frac{k_5 \ll mod(k_{37}, 8) + k_6 \ll mod(k_{38}, 8) + k_7 \gg mod(k_{39}, 8) + k_8 \gg mod(k_{40}, 8)}{4 * 256 + 1} \\ d_3 = \frac{k_9 \gg mod(k_{41}, 8) + k_{10} \gg mod(k_{42}, 8) + k_{11} \gg mod(k_{43}, 8) + k_{12} \gg mod(k_{44}, 8)}{4 * 256 + 1} \\ d_4 = \frac{k_{13} \ll mod(k_{45}, 8) \oplus k_{14} \ll mod(k_{46}, 8) \oplus k_{15} \ll mod(k_{47}, 8) \oplus k_{16} \ll mod(k_{48}, 8)}{256 + 1} \\ d_5 = \frac{k_{17} \gg mod(k_{49}, 8) \oplus k_{18} \gg mod(k_{50}, 8) \oplus k_{19} \gg mod(k_{51}, 8) \oplus k_{20} \gg mod(k_{52}, 8)}{256 + 1} \\ d_6 = \frac{k_{21} \gg mod(k_{53}, 8) + k_{22} \ll mod(k_{54}, 8) \oplus k_{23} \ll mod(k_{55}, 8) \oplus k_{24} \ll mod(k_{56}, 8)}{2 * 256 + 1} \\ d_7 = \frac{k_{25} \gg mod(k_{57}, 8) \oplus k_{26} \gg mod(k_{58}, 8) \oplus k_{27} \gg mod(k_{59}, 8) + k_{28} \ll mod(k_{60}, 8)}{2 * 256 + 1} \\ d_8 = \frac{k_{29} \gg mod(k_{61}, 8) \oplus k_{30} \gg mod(k_{62}, 8) + k_{31} \ll mod(k_{63}, 8) \oplus k_{32} \ll mod(k_{64}, 8)}{2 * 256 + 1} \end{array} \right. \quad (15)$$

where \ll represents a cyclic left shift to the binary sequence, \gg represents a cyclic right shift to a binary sequence, and \oplus represents the exclusive-or operator.

3.1.2. Sum of Plaintext Image Pixel Values $sumP$

Accumulate and sum all pixel values of the plaintext image to obtain the key $sumP$, whose expression is Equation (16):

$$sumP = \sum_{x=1}^m \sum_{y=1}^n P(x, y) \quad (16)$$

where $P(x, y)$ represents the pixel value at the (x, y) position.

3.1.3. Image block size $Bsize$

First, select the short side of the image, and assume M is the short side. Then, divide M by an odd number within 11~30, and select the odd number corresponding to the number with the largest fractional part from the result as the block size $Bsize$.

3.1.4. Supplementary Parameters $M1$, $N1$ and Number of Blocks $Bnum$

According to the block size $Bsize$, the rows and columns of the image are filled with numbers that are divisible by $Bsize$, and the number of rows $M1$ and the number of columns $N1$ of the supplementary element 0 are used as the key. The calculation formula is Equation (17):

$$M1 = mod(M, Bsize); N1 = mod(N, Bsize) \quad (17)$$

where mod represents the modulo, M and N are the number of rows and columns of the original image, and $Bsize$ is the block size.

After adding elements to the original image, its row and column are $M2$ and $N2$, and the number of blocks is calculated by the following Equation (18):

$$Bnum = \frac{M2}{Bsize} * \frac{N2}{Bsize} \quad (18)$$

3.2. Generating 3D Probability Magnitude Matrix, 3D Probability Distribution Matrix, and 3D Quantum Hash Sequence by Using Quantum Walks

We used a one-dimensional quantum walk to generate a one-dimensional probability distribution sequence, then encoded the probability distribution sequence to generate a quaternary message and performed controlled alternating quantum walks by encoding the message. Finally, it generated the probability amplitude matrix and probability distribution matrix of multiple CAQWs by combining a 3D probability amplitude matrix and 3D probability distribution matrix and then generated a 3D quantum hash sequence according to the probability distribution matrix. We applied the generated one-dimensional probability distribution sequence, 3D probability amplitude matrix, 3D probability distribution matrix, and 3D quantum hash sequence to the three-dimensional cuboid image encryption algorithm.

3.2.1. Generation of Initial Parameters for 1DQWs

(1) Number of nodes on the circle

According to the key $sumP$ generated in Section 3.1.2, the ten-digit number SP of the sum of pixel values is calculated by Equation (19). Then calculate the length l_{mess} of the message through the parameter d_1 in Section 3.1.1, as shown in Equation (20). If $sumP = 0$, then the length of the message l_{mess1} is Equation (21). Finally, the number of nodes TC of the circle is given by Equation (22).

$$SP = floor(\log_{10}sumP) \quad (19)$$

$$l_{mess} = \text{mod}(\text{floor}(\text{sumP} * d_1 * 10^{15-SP}), 2^5) + 1 + Bsize \quad (20)$$

$$l_{mess1} = 13 + Bsize \quad (21)$$

$$TC = l_{mess1} * Bnum \quad (22)$$

where floor means rounding down, \log_{10} is a logarithmic function with base 10, and mod means a modulo operation.

(2) Coin parameter θ

The coin parameter θ is calculated by the parameter d_2 of Section 3.1.1, as shown in Equation (23).

$$\theta = \text{mod}(d_2 * 10^{15} * (\frac{\pi}{7} + 2), \frac{\pi}{2}) \quad (23)$$

where mod represents the modulo operation.

(3) The initial state of the coin

The initial state of the coin is $\alpha|0\rangle + \beta|1\rangle$. We used the parameters d_3 and d_4 in Section 3.1.1 to generate the initial state of the coin $\alpha, \beta, \alpha, \beta$ is expressed as the following Equation (14). Because the coin operator needs to satisfy $|\alpha|^2 + |\beta|^2 = 1$, we constructed the quadratic equation of one variable of Equation (25) to calculate the initial state of the generated coins.

$$\alpha = d_3 + (\frac{d_3}{2})i; \beta = (\frac{d_4}{2}) + xi \quad (24)$$

$$f = 1 - \left(\sqrt{d_3^2 + (\frac{d_3}{2})^2} \right)^2 - \left(\sqrt{(\frac{d_4}{2})^2 + x^2} \right)^2 = 0 \quad (25)$$

where α, β are the amplitude and phase of the initial state (complex number), i represents the complex unit, f represents the quadratic equation to be solved, and x represents the unknown parameter.

3.2.2. Generation of Initial Parameters of CAQWs

- (1) The number of nodes on the circle of CAQWs is equal to the block size $Bsize$.
- (2) Coin parameters θ_0, θ_1

The coin parameters θ_0, θ_1 are calculated by the parameters d_7 and d_8 in Section 3.1.1, as shown in Equations (26) and (27)

$$\theta_0 = \text{mod}(d_7 * 10^{15} + (\frac{\pi}{5} + 2), \frac{\pi}{2}) \quad (26)$$

$$\theta_1 = \text{mod}(d_8 * 10^{15} + (\frac{\pi}{5} + 0.1), \frac{\pi}{2}) \quad (27)$$

(3) Initial state of the coin

Similar to the initial state of the coin of 1DQWs, the expressions of $\alpha1, \beta1$ are Equation (28). Because the coin operator needs to satisfy $|\alpha1|^2 + |\beta1|^2 = 1$, we constructed the quadratic equation of one variable of Equation (29) to calculate the initial state of the generated coins.

$$\alpha1 = (\frac{d_5}{2}) + (\frac{d_5}{3})i; \beta1 = (\frac{d_6}{2}) + x1i \quad (28)$$

$$f1 = 1 - \left(\sqrt{(\frac{d_5}{2})^2 + (\frac{d_5}{3})^2} \right)^2 - \left(\sqrt{(\frac{d_6}{2})^2 + x1^2} \right)^2 = 0 \quad (29)$$

where $\alpha1, \beta1$ are the amplitude and phase of the initial state (complex number), i represents the complex unit. $f1$ represents the quadratic equation to be solved, and $x1$ represents the unknown parameter.

3.2.3. Generating Probability Distribution Sequences Using 1DQWs

According to the initial parameters, we performed a 1D discrete quantum walk [38]. After t steps, the probability of finding a walker at position x is Equation (30), and we denoted this sequence of probability distributions as $Qum1D$.

$$P(x, t) = \sum_{c \in \{0,1\}} |\langle x, c | (\hat{M})^t | \psi \rangle_0|^2 \quad (30)$$

where $P(x, t)$ represents the probability of finding a walker at x after t steps.

3.2.4. Message Encoding

We mapped the probability distribution sequence $Qum1D$ generated by 1DQWs to values 0–255, as shown in Equation (31), and quaternary encoded it and the encoded message as the message.

$$\text{message} = \text{mod}(\text{mod}(\text{floor}(Qum1D * 10^{200}), 256), 4) \quad (31)$$

where mod represents the modulo operation, and floor represents the rounding down.

3.2.5. Controlled Alternate Quantum Walks for Message Encoding

In the proposed image encryption algorithm, we improved the two-dimensional controlled alternating walk model and encoded the sequence generated by 1DQWs into a quaternary sequence as a control message. We also applied the quaternary message encoding to the evolution process of the quantum system [40] by using Equation (32) to represent the global unitary operators $\hat{M}_0, \hat{M}_1, \hat{M}_2, \hat{M}_3$.

$$\begin{cases} \hat{M}_0 = \hat{N}_y(\hat{I} \otimes \hat{O}_0)\hat{N}_x(\hat{I} \otimes \hat{O}_0) \\ \hat{M}_1 = \hat{N}_y(\hat{I} \otimes \hat{O}_0)\hat{N}_x(\hat{I} \otimes \hat{O}_1) \\ \hat{M}_2 = \hat{N}_y(\hat{I} \otimes \hat{O}_1)\hat{N}_x(\hat{I} \otimes \hat{O}_0) \\ \hat{M}_3 = \hat{N}_y(\hat{I} \otimes \hat{O}_1)\hat{N}_x(\hat{I} \otimes \hat{O}_1) \end{cases} \quad (32)$$

Assuming that the message string generated by 1DQWs is “320102”, the state of the entire system can be expressed as Equation (33):

$$|\psi\rangle_6 = \hat{M}_2 \hat{M}_0 \hat{M}_1 \hat{M}_0 \hat{M}_2 \hat{M}_3 |\psi\rangle_0 \quad (33)$$

After t steps, the final state of the entire quantum system is Equation (34):

$$|\psi\rangle_t = (\hat{M})^t |\psi\rangle_0 \quad (34)$$

After t steps, the probability amplitude of finding a walker at position (x, y) is Equation (35), and the probability is Equation (36):

$$F(x, y, t) = \sum_{c \in \{0,1\}} \langle x, y, c | (\hat{M})^t | \psi \rangle_0 \quad (35)$$

$$P(x, y, t) = \sum_{c \in \{0,1\}} |\langle x, y, c | (\hat{M})^t | \psi \rangle_0|^2 \quad (36)$$

3.2.6. Three-Dimensional Probability Amplitude Matrix and Three-Dimensional Probability Distribution Matrix

According to the number of blocks $Bnum$ in Section 3.1.4, we divided the message encoding message into $Bnum$ groups and used Section 3.2.2 to calculate the generated initial parameters of the system. According to the corresponding message encoding, we performed $Bnum$ times of message encoding-controlled alternate quantum walks on the

circle and finally generated a 3D probability amplitude matrix fre of size $2 * (Bsize * Bsize) * Bnum$, whose expression is Equation (37). At the same time, a 3D probability distribution matrix $Qum2D$ of size $Bsize * Bsize * Bnum$ was generated, and its expression is Equation (38).

$$fre(2, Bsize * Bsize, i) = \varphi(F(x, y, t), message(i))i = 1, \dots, Bnum \quad (37)$$

where $\varphi(F(x, y, t), message(i))$ represents the probability amplitude matrix which generated under the control of the $i - th$ group of $message$ encoding messages.

$$Qum2D(Bsize, Bsize, i) = \omega(P(x, y, t), message(i))i = 1, \dots, Bnum \quad (38)$$

where $\omega(P(x, y, t), message(i))$ represents the probability matrix which generated under the control of the $i - th$ group of $message$ encoding messages.

3.2.7. Three-Dimensional Quantum Hash Sequence

Quantum hash sequences have chaotic-dynamics-like properties and can be used to generate pseudorandom numbers. We converted the 3D probability distribution matrix $Qum2D$, which was generated in Section 3.2.6, into a binary string using Equations (39) and (40) and finally obtained the 3D quantum hash sequence $Btest$. In the diffusion stage, we used the 3D quantum hash sequence $Btest$ to complete the diffusion operation.

$$B = mod(floor(Qum2D * 10^{15}), 256) \quad (39)$$

$$Btest = dec2bin(B) \quad (40)$$

where $dec2bin$ means converting a decimal number to binary.

3.3. Image Encryption Process

Combining the discrete quantum walk model, we propose a three-dimensional cuboid image encryption algorithm with two rounds of scrambling and two rounds of diffusion operations. First, we used 1DQWs to generate a probability value sequence $Qum1D$, then encoded $Qum1D$ into a quaternary message $message$. Then, we used the encoded message to control the alternate quantum walk model to generate a 3D probability amplitude matrix and 3D probability distribution matrix. Finally, we used the 3D probability distribution matrix obtain the 3D quantum hash series. The operation is shown in Algorithm 1. We used the probability value sequence $Qum1D$ and 3D probability distribution matrix to complete the image scrambling and used the 3D probability magnitude matrix and 3D quantum hash series to diffuse the image to obtain the final encrypted image. The operation is shown in Algorithm 2. The following are the specific steps of our proposed encryption scheme, and its flow chart is shown in Figure 3.

Algorithm 1. Sequence generation.

```

Input: Original image(PlainImg)
Output:  $d_1 \sim d_8, Qum1D, message, fre, Qum2D, Btest$ 
1  $k_1 \sim k_{64} \leftarrow \text{SHA-512}(PlainImg)$ 
2  $d_1 \sim d_8 \leftarrow \text{Generate initial key parameters based on } k_1 \sim k_{64}$ 
3 Calculation of 1DQWs and 2DCAQWs
4  $Qum1D \leftarrow \text{1DQWs}(TC, t, \theta, \alpha, \beta) // 1\text{DQWs on a circle with node number } TC$ 
5  $message \leftarrow \text{encoding}(Qum1D) // \text{Quadratic encoding}$ 
6  $fre(2, Bsize * Bsize, i) \leftarrow \varphi(F(x, y, t), message(i))i = 1, \dots, Bnum;$ 
7  $Qum2D(Bsize, Bsize, i) \leftarrow \omega(P(x, y, t), message(i))i = 1, \dots, Bnum // \text{Alternating quantum walks with } Bnum \text{ sub-message encoding control on a circle}$ 
8  $Btest \leftarrow dec2bin(Qum2D) // \text{Complete diffusion operation using 3D quantum hash sequence Btest}$ 

```

Algorithm 2. Encryption algorithms.

Input: Original image(PlainImg), Qum1D, message, fre, Qum2D, Btest
Output: Encrypted images(En)

- 1 Image block ($Bsize * Bsize * Bnum$) \leftarrow chunking the image
- 2 Plain3D \leftarrow Integrating image blocks as rectangles
- 3 prm1Dt \leftarrow sum(reshape(Qum1D, lmess, Bnum)); // Group summation
- 4 $[\sim, prm1Dindex] \leftarrow sort(prm1Dt)$ // Sort
- 5 PrmP3D \leftarrow Displacement between layers according to its index sequence $prm1Dindex$ for the image rectangle Plain3D
- 6 Prm2 \leftarrow Sorting and dislocation inside each depth layer using Qum2D
- 7 for j \leftarrow 1 to B_num
- 8 BinP3 = dec2bin(Prm2);
- 9 for i \leftarrow 1 to x * y do
- 10 BinP3_t \leftarrow reshape(BinP3)
- 11 If A > B
- 12 Bin_P3 \leftarrow rot90(BinP3_t Upper) // Upper layer rotated 90 degrees counterclockwise
- 13 else
- 14 Bin_P3 \leftarrow rot90(BinP3_t Lower) // Lower layer rotated clockwise by 90 degrees
- 15 end
- 16 P3bin(i,:) = reshape(Bin_P3);
- 17 end
- 18 P3bin1 = bin2dec(P3bin);
- 19 P3bin2 = reshape(P3bin1, x, y);
- 20 end
- 21 Ctest = bitxor(Btest, P3bin2) // Global xor
- 22 En \leftarrow Tiling the image block Ctest

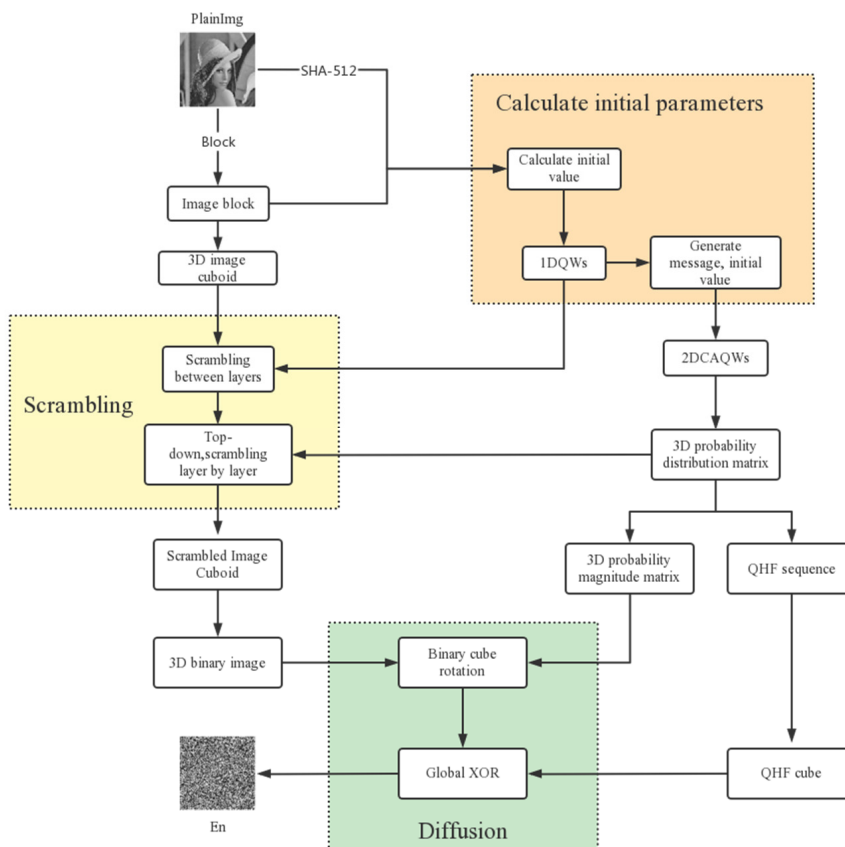


Figure 3. A 3D Cuboid Image Encryption Framework Based on Message-Encoded Controlled Alternate Quantum Walks.

3.3.1. Generation of Image Cuboid

Step one: Image segmentation

According to the supplementary parameters $M1$ and $N1$ generated in Section 3.1.4, the plaintext image blocks were supplemented with zero elements in row $M1$ and column $N1$, and then according to the image block size $Bsize$ generated in Section 3.1.3 and the number of blocks $Bnum$ generated in Section 3.1.4, we divided the filled image into image blocks whose size is $Bsize * Bsize$, $Bnum$ number.

Step two: Combine into a 3D image cuboid

The $Bnum$ image blocks generated by Step One were converted into a three-dimensional image cuboid $plain3D$ with the size of $Bsize * Bsize * Bnum$, line by line, from left to right, and from top to bottom, as shown in Figure 4.

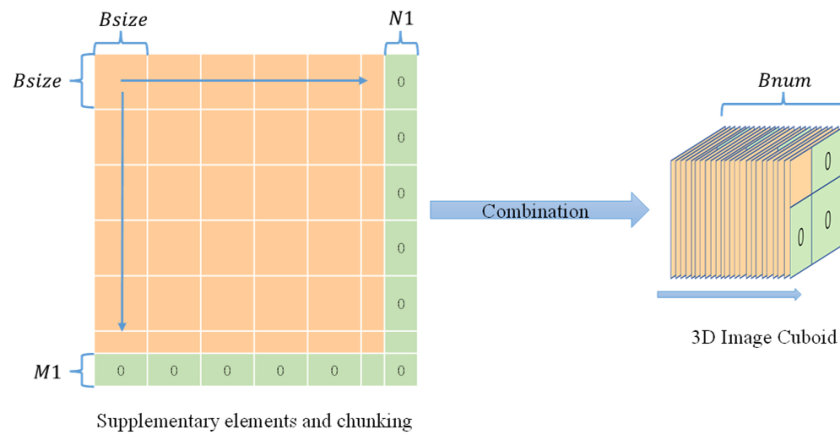


Figure 4. Generation of image cuboid.

3.3.2. Two Rounds of Scrambling

Step one: Interlayer scrambling based on one-dimensional quantum walk.

According to Equation (41), we divided the probability distribution sequence $Qum1D$ generated in Section 3.2.3 into $Bnum$ groups and then summed the sequences of each group to obtain the sequence $prm1Dt$. The operation process is shown in Figure 5.

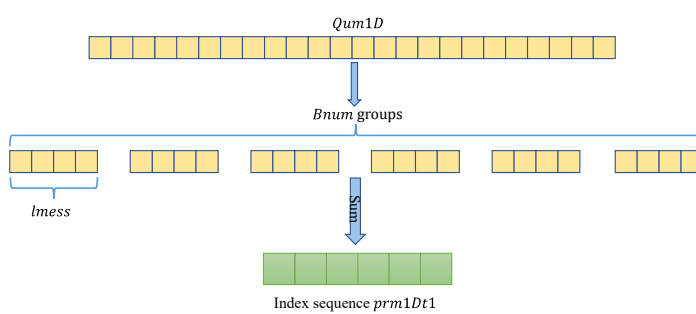


Figure 5. Generation of index sequence $prm1Dt$.

Then, Equation (42) was used to sort $prm1Dt$ from small to large, and the image cuboid $Plain3D$ was scrambled between layers according to its index sequence $prm1Dindex$ to obtain the scrambled image block $PrmP3D$ between layers, as shown in Figure 6.

$$prm1Dt = \text{sum}(\text{reshape}(Qum1D, lmess, Bnum)) \quad (41)$$

where reshape is an array reconstruction function, $lmess$ represents the message length, $Bnum$ represents the number of blocks, and sum represents the sum of the array by columns.

$$[\sim, prm1Dindex] = \text{sort}(prm1Dt) \quad (42)$$

where $sort$ is the sorting function and $prm1Dindex$ is the sequence of index sorting.

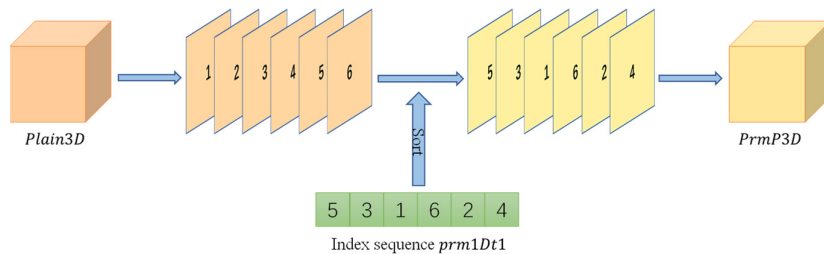


Figure 6. Interlayer scrambling of image cuboids.

Step Two: Layer-by-layer scrambling based on 3D probability distribution matrix

The three-dimensional probability distribution matrix $Qum2D$ generated in Section 3.2.6 sorted the image block from smallest to largest in order from top to bottom in each depth layer and used the index sort matrix generated at each layer. The image block $PrmP3D$ was scrambled layer by layer to obtain a new image block $Prm2$, as shown in Figure 7.

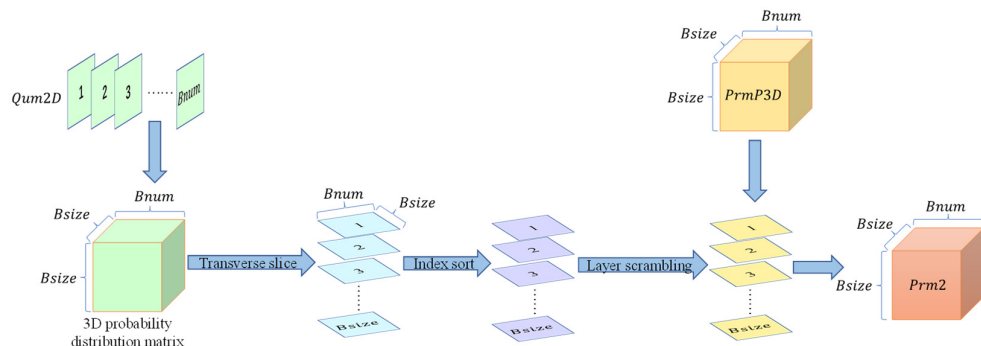


Figure 7. Top-down layer-by-layer scrambling based on 3D probability distribution matrix.

3.3.3. Two Rounds of Diffusion

Step one: Binary cube rotation based on probability magnitude matrix

As shown in Figure 8, each 0–255 pixel value of the image block $Prm2$ obtained by scrambling in Section 3.3.2 was operated from left to right, layer by layer. Then, we operated it from back to front and top to bottom and encoded as a binary cube. According to the 3D probability amplitude matrix obtained in Section 3.2.6, the binary cube was rotated. We divided the probability amplitude into A direction and B direction. If $A > B$, the upper layer of the binary cube was rotated 90 degrees counterclockwise; otherwise, the lower layer of the binary cube was rotated 90 degrees clockwise. Finally, the binary cube corresponding to each pixel value was converted into a binary sequence, and we obtained the 3D image block $P3bin$ after the binary cube rotation operation.

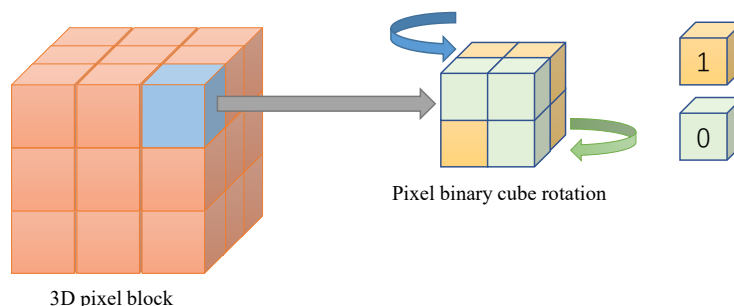


Figure 8. Binary cube rotation based on probability magnitude matrix.

Step two: Diffusion based on 3D quantum hash sequence

By using the 3D quantum hash series $Btest$ obtained in Section 3.2.7, we performed a global bitwise XOR operation with the 3D image block $P3bin$ according to Equation (43). We converted it into a decimal sequence and obtained the image block $Ctest$. Then, we tiled the image block $Ctest$ to obtain the final encrypted image En .

$$Ctest = bitxor(Btest, P3bin) \quad (43)$$

where $bitxor$ means bitwise exclusive or.

3.4. Image Decryption Process

The image decryption process is the reverse operation of the encryption process, and the steps are as follows:

Step one: According to the key $Bsize$ in Section 3.1.3 and the key $Bnum$ in Section 3.1.4, we divided the encrypted image En into blocks and then combined them into cubes $De3D$.

Step two: We converted each pixel value of the cube $De3D$ into a binary sequence and performed a global bitwise XOR operation with the 3D quantum hash series $Btest$ which was obtained in Section 3.2.7 to acquire the image block $De1$.

Step three: Each pixel value of image block $De1$ was encoded into a binary cub, and a reverse rotation operation was performed on the binary cube according to the three-dimensional probability amplitude matrix obtained in Section 3.2.6. This operation is a reverse of Section 3.3.3, resulting in an image block $De2$.

Step four: The 3D probability distribution matrix $Qum2D$ generated in Section 3.2.6 was sorted by index for each layer, in the order from the top to the bottom. The image block $De2$ was inversely indexed and scrambled layer by layer according to the index order to obtain $De3$.

Step five: According to the index $prm1Dindex$ generated in Section 3.3.2, $De3$ was scrambled with interlayer inverse index to obtain $De4$.

Step six: By tiling the image block $De4$ obtained in the previous step and removing the supplementary zero elements by row and column according to the keys $M1$ and $N1$ obtained in Section 3.1.4, we obtained the final decrypted image De .

4. Simulation Results and Security Analysis

In order to test the security performance of the proposed image encryption scheme, we used MATLAB R2020b software to conduct simulation experiments on a computer with Windows 10 system, 16 GB memory, and i5-10500 CPU. The images we used in testing included 256 * 256 square images (Lena, Baboon, Peppers, White, Black), 512 * 512 square images (Barbara, Cameraman, Livingroom), irregular Lena image, and images from standard 25 grayscale images of the USC-SIPI image database.

4.1. Encryption and Decryption Results

In this paper, 256 * 256, 512 * 512 square images and irregular Lena image were used for testing. The test results of 256 * 256 images (Lena, Baboon, Peppers, White, Black) are shown in Figure 9. The encryption and decryption results of 512 * 512 images (Barbara, Cameraman, Livingroom) and irregular Lena images are shown in Figure 10. The encrypted images shown in the figure cannot show any meaningful information, and the original images with rich information can be obtained by decrypting with the correct key.

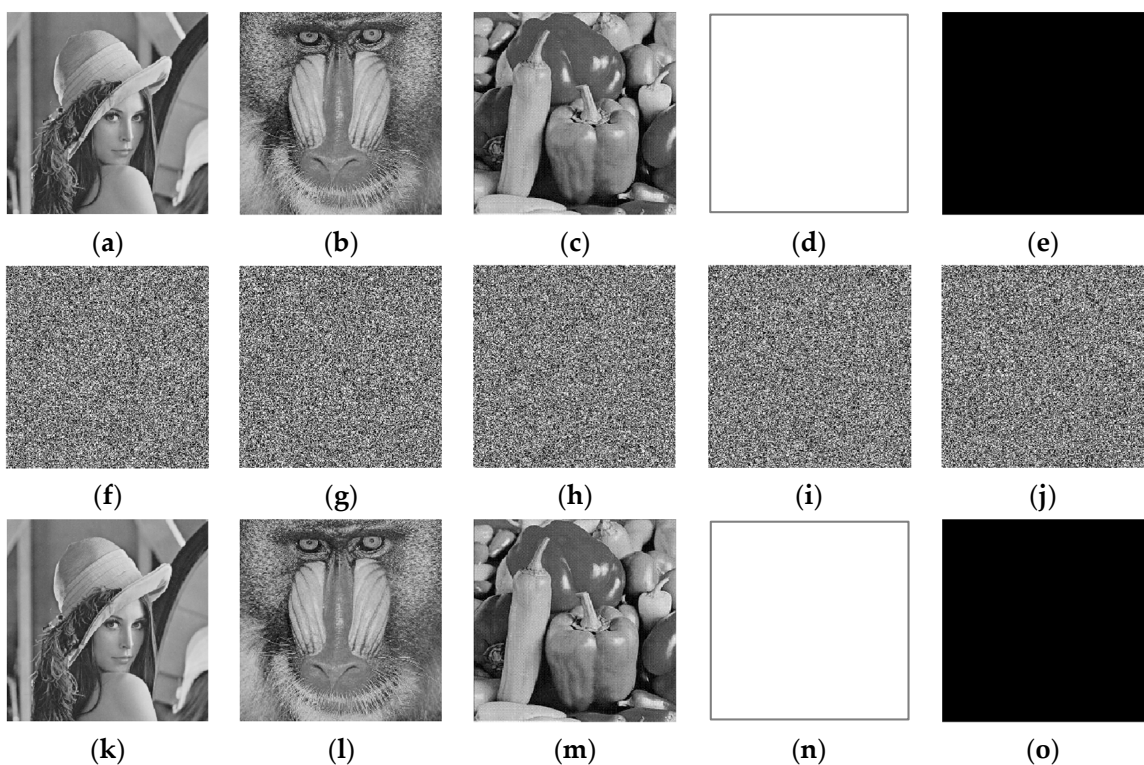


Figure 9. Simulation results (256×256): (a–e) original images; (f–j) encrypted images; (k–o) decrypted images.

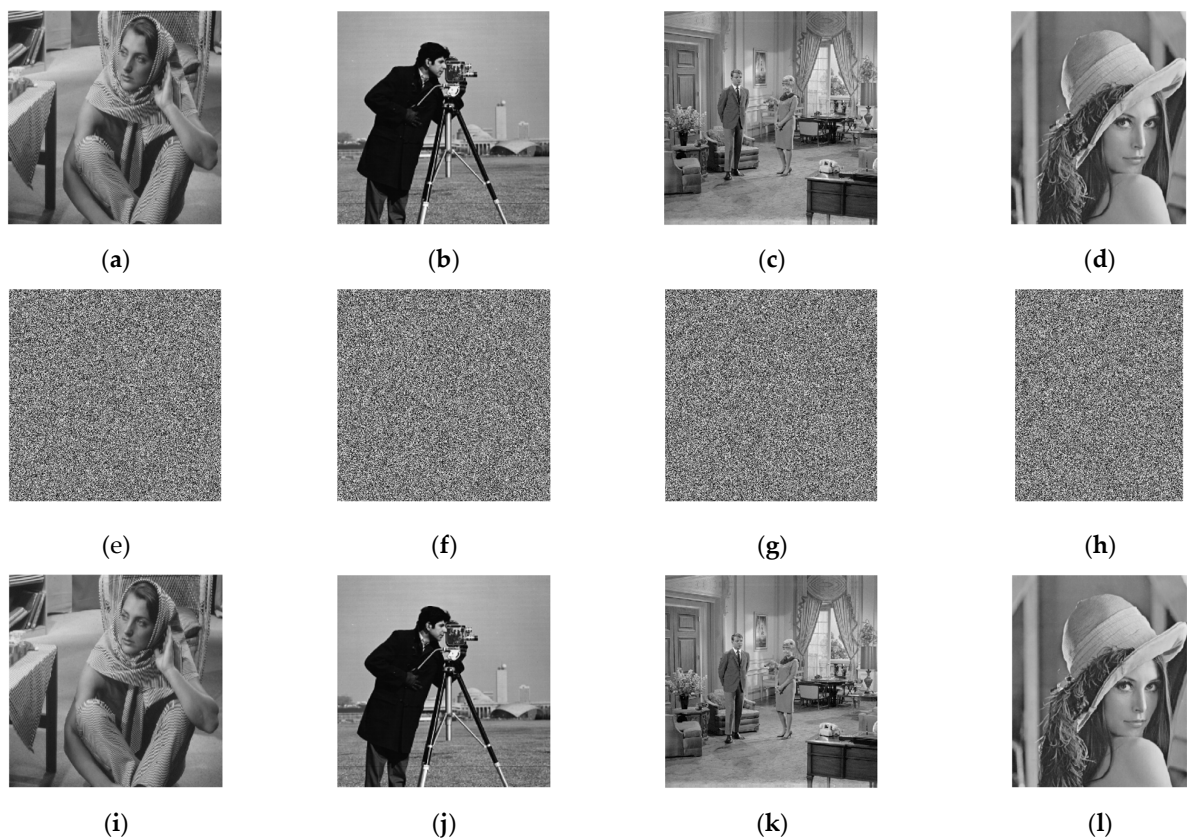


Figure 10. Simulation results (512×512 and irregular): (a–d) original images; (e–h) encrypted images; (i–l) decrypted images.

4.2. Histogram Analysis

The pixel histogram shows the distribution of different pixel values in the image. We tested and analyzed the histogram of encrypted images. The histogram analysis results of 256×256 size images are shown in Figure 11, and the histogram analysis results of 512×512 size images and irregular Lena image are shown in Figure 12. It can be seen that the distribution frequency of pixel values in the encrypted images is relatively uniform, and the trend of the histogram is stable, which has a good ability to resist statistical attacks.

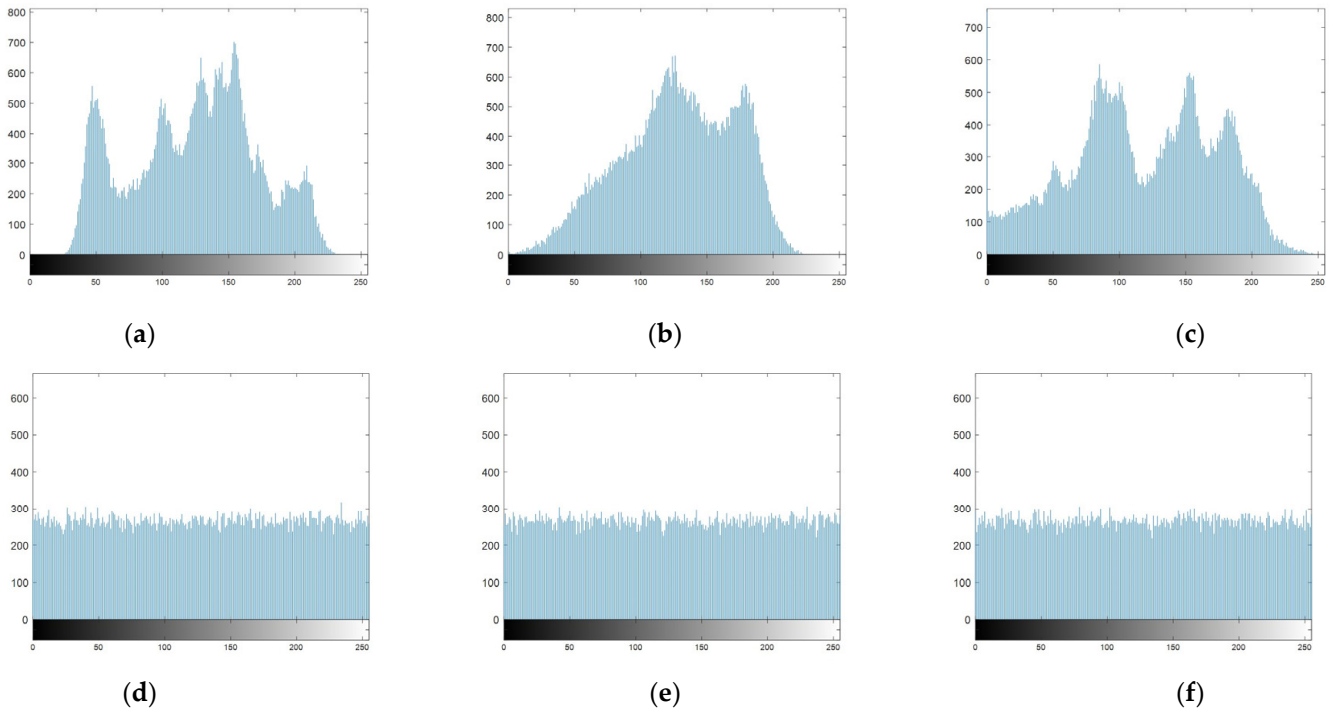


Figure 11. Histogram Analysis (256×256): (a–c) original images; (d–f) encrypted image.

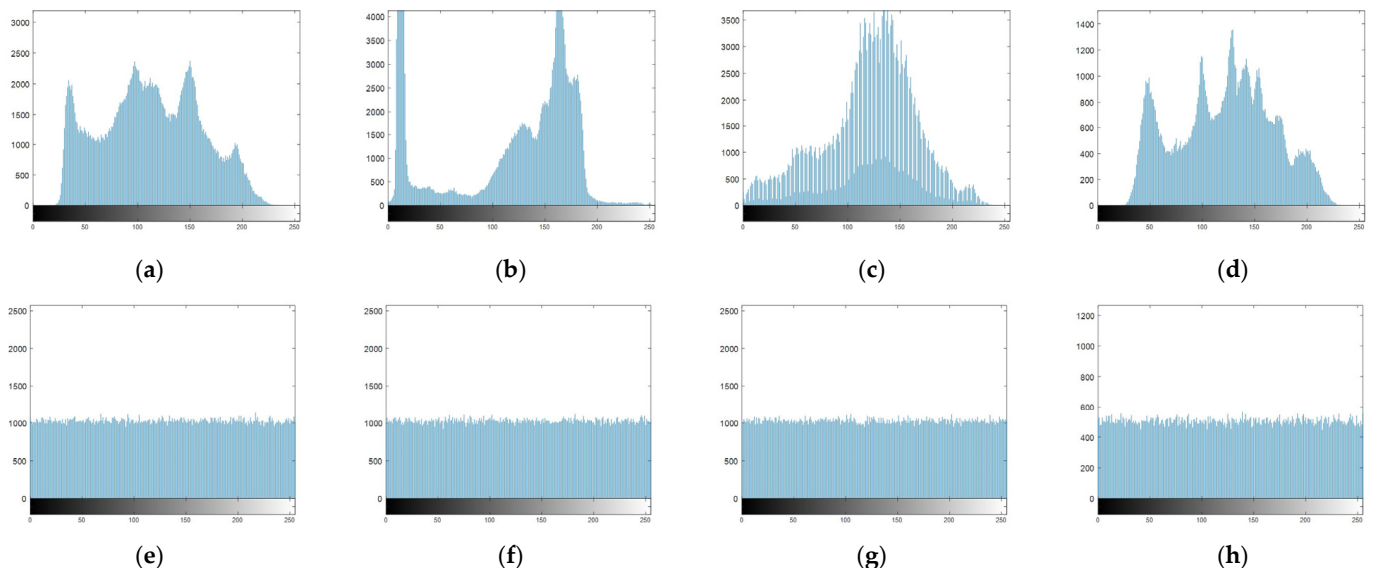


Figure 12. Histogram Analysis (512×512 and irregular): (a–d) original images; (e–h) encrypted image.

4.3. χ^2 Test

We use the χ^2 test to describe the distribution of the pixel histogram [42], whose formula is Equation (44):

$$\chi^2 = \sum_{i=1}^{255} \frac{(v_i - v_0)^2}{v_0} \quad (44)$$

where χ^2 represents the value of the chi-square test, i represents the pixel value, v_i represents the frequency of the pixel value i in the image, and v_0 represents the expected frequency of the pixel value i , $v_0 = (M * N) / 256$. The smaller the value of the χ^2 test, the more uniform the pixel distribution. When the confidence is $\alpha = 0.05$, the condition for passing the test is that χ^2 is less than 293.24783.

Table 1 (Lena, Baboon, Peppers, White, Black) and Table 2 (Barbara, Cameraman, Livingroom, Irregular Lena) show the test results of plaintext images and the results in comparison with others' methods. The images were encrypted with different sizes, and all results passed the test conditions, which shows that our algorithm has a good ability to resist statistical attacks.

Table 1. χ^2 test (256 * 256).

Image	Lena	Baboon	Peppers	White	Black	Avg.	Ref. [9]	Ref. [33]
Plaintext	39,868.727	44,739.305	26,311.578	16,711,680	16,711,680	-	-	-
Ciphertext	219.269	216.589	225.765	259.881	241.390	232.579	244.159	254.078

Table 2. χ^2 test (512 * 512 and irregular).

Image	Barbara	Cameraman	Livingroom	Irregular Lena	Avg.	Ref. [18]
Plaintext	14,4101.119	418,530.147	276,815.883	74,075.357	-	-
Ciphertext	238.454	250.778	245.376	250.828	246.359	260.400

4.4. Correlation Coefficient Analysis

There is a strong correlation between the adjacent pixels of the original image, and the lower the correlation of the ciphertext image, the stronger the resistance of the algorithm to statistical attacks. The calculation formula of pixel correlation is such as Equations (45)–(47):

$$r_{xy} = \frac{E((x - E(x))(y - E(y)))}{\sqrt{D(x)D(y)}} \quad (45)$$

$$E(x) = \frac{1}{N} \sum_{i=1}^N x_i \quad (46)$$

$$D(x) = \frac{\sum_{i=1}^n (x_i - E(x))^2}{N} \quad (47)$$

where r_{xy} is the pixel correlation coefficient, and $E(x)$ and $D(x)$ are the expectation and variance.

We selected 2000 pairs of pixels on the horizontal, vertical, and diagonal lines of the image for 30 tests and took the average value. Figure 13 shows the correlation distribution of the horizontal, vertical, and diagonal lines of the images in the USC-SIPI image database, and their values all hovered around zero. For example, the correlations in the horizontal, vertical, and diagonal directions are shown in Figures 14–16. Table 3 shows the results of ours and the comparison with others' methods, bold indicates the average of pixel correlation coefficients in different directions of the image, and the pixel correlation coefficient is much lower than that of the plaintext image, which fully shows that our method has strong resistance to statistical analysis.

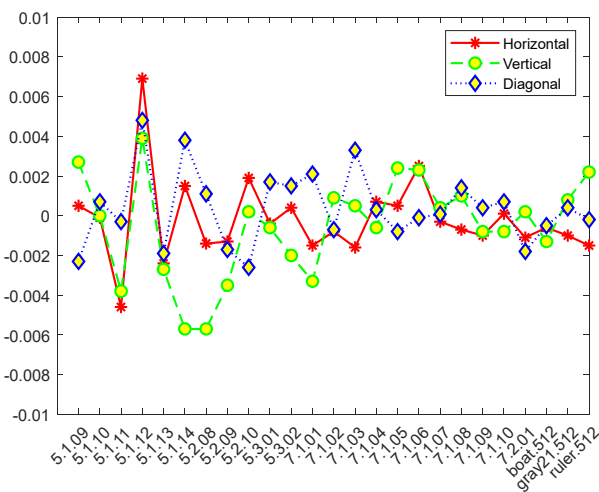


Figure 13. Correlation of different ciphertext images.

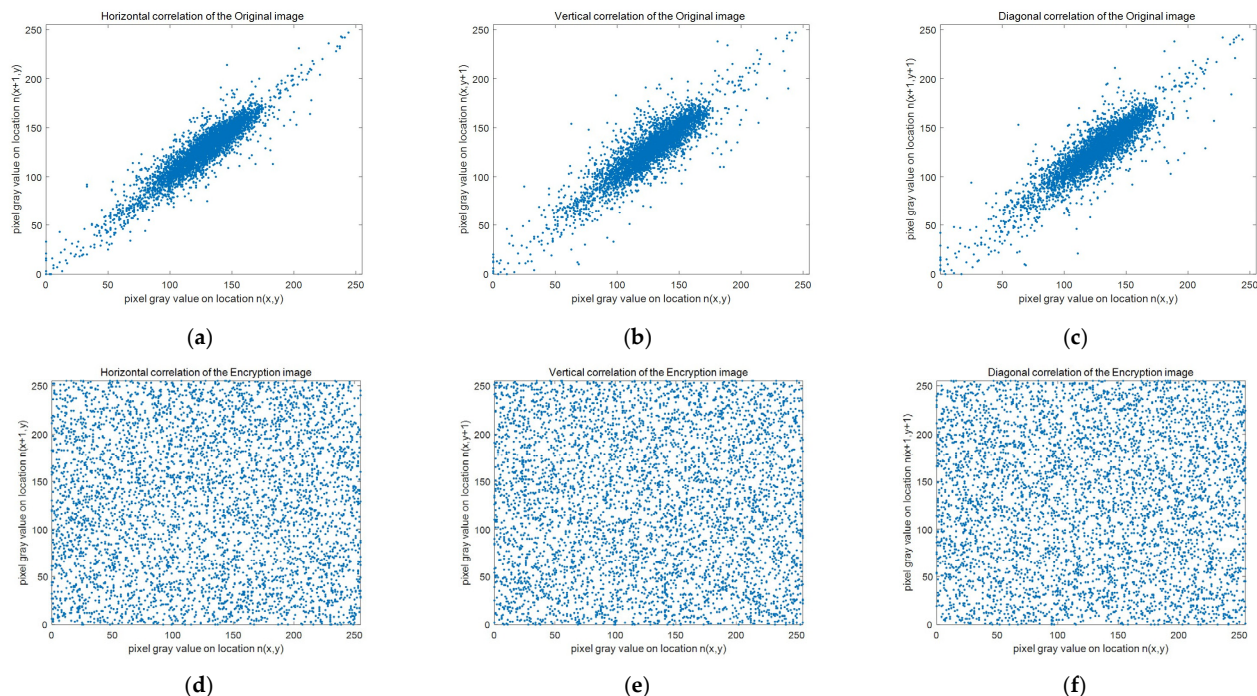


Figure 14. Adjacent pixel correlation of image 5.1.09: (a–c) original image; (d–f) encrypted image.

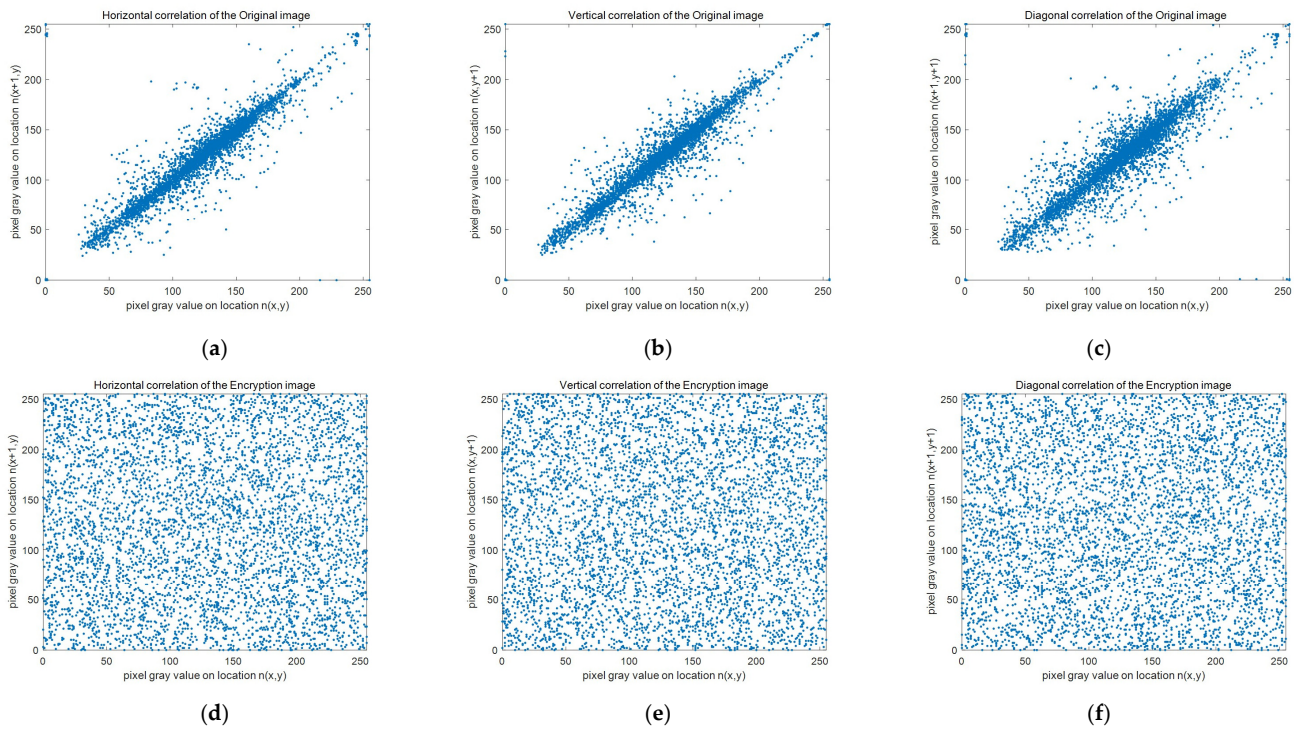


Figure 15. Adjacent pixel correlation of image 5.2.08: (a–c) original image; (d–f) encrypted image.

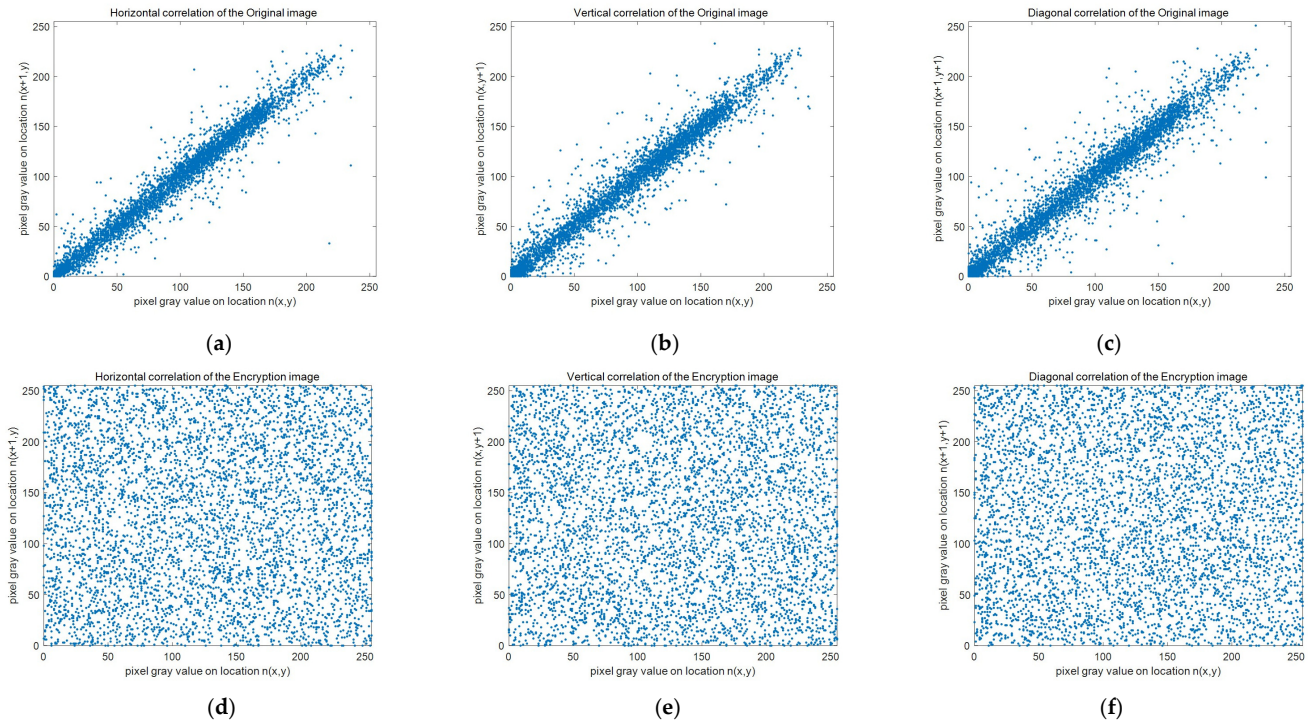


Figure 16. Adjacent pixel correlation of image 5.3.01: (a–c) original image; (d–f) encrypted image.

Table 3. Pixel correlation in different directions.

Image	Plain Image			Cipher Image			Ref. [11]		
	H	V	D	H	V	D	H	V	D
5.1.09	0.9026	0.9406	0.9098	0.0005	0.0027	-0.0023	0.0031	-0.0016	0.0014
5.1.10	0.9016	0.8688	0.8311	-0.0001	1.0819×10^{-6}	0.0007	0.0044	-0.0006	-0.0052
5.1.11	0.9574	0.9480	0.8966	-0.0046	-0.0038	-0.0003	0.0005	-0.0019	-0.0049
5.1.12	0.9576	0.9741	0.9408	0.0069	0.0039	0.0048	0.0068	-0.0002	-0.0055
5.1.13	0.8804	0.8497	0.7419	-0.0024	-0.0027	-0.0019	5.76×10^{-6}	0.0017	-0.0072
5.1.14	0.9522	0.9018	0.8589	0.0015	-0.0057	0.0038	-0.0056	0.0001	0.0044
5.2.08	0.9289	0.8784	0.8472	-0.0014	-0.0057	0.0011	0.0028	0.0006	-0.0027
5.2.09	0.9059	0.8701	0.8122	-0.0013	-0.0035	-0.0017	0.0006	-0.0123	0.0001
5.2.10	0.9409	0.9274	0.8948	0.0019	0.0002	-0.0026	-0.0024	-0.0005	0.0031
5.3.01	0.9756	0.9811	0.9669	-0.0004	-0.0006	0.0017	0.0015	4.43×10^{-5}	-0.0017
5.3.02	0.9154	0.9053	0.8608	0.0004	-0.0020	0.0015	-0.0024	-0.0011	0.0008
7.1.01	0.9635	0.9194	0.9080	-0.0015	-0.0033	0.0021	-0.0021	0.0011	0.0067
7.1.02	0.9468	0.9478	0.9032	-0.0008	0.0009	-0.0007	0.0084	0.0017	0.0021
7.1.03	0.9410	0.9306	0.8998	-0.0016	0.0005	0.0033	0.0045	8.67×10^{-5}	-0.0056
7.1.04	0.9762	0.9646	0.9546	0.0007	-0.0006	0.0003	-0.0031	0.0073	0.0002
7.1.05	0.9449	0.9193	0.8983	0.0005	0.0024	-0.0008	-0.0040	-0.0004	-0.0002
7.1.06	0.9378	0.9004	0.8791	0.0025	0.0023	-0.0001	0.0002	-0.0014	-0.0057
7.1.07	0.8872	0.8735	0.8296	-0.0003	0.0004	7.5782×10^{-5}	0.0020	-0.0009	-0.0160
7.1.08	0.9563	0.9335	0.9245	-0.0007	0.0010	0.0014	0.0083	-0.0008	0.0057
7.1.09	0.9667	0.9277	0.9160	-0.0010	-0.0008	0.0004	0.0007	-0.0005	0.0063
7.1.10	0.9659	0.9497	0.9341	0.0001	-0.0008	0.0007	0.0058	-0.0001	0.0050
7.2.01	0.9670	0.9468	0.9463	-0.0011	0.0002	-0.0018	-0.0008	-0.0031	-0.0044
boat.512	0.9371	0.9722	0.9220	-0.0006	-0.0013	-0.0005	0.0024	-6.53×10^{-7}	-0.0036
gray21.512	0.9965	0.9998	0.9963	-0.0010	0.0008	0.0004	0.0011	0.0007	-0.0056
ruler.512	0.4332	0.5068	-0.0207	-0.0015	0.0022	-0.0002	0.0007	0.0120	3.59×10^{-5}
Mean	0.9215	0.9095	0.8581	-0.0014	0.0019	0.0014	0.0013	0.0020	0.0042

4.5. Information Entropy Analysis

Information entropy can be used to measure the randomness of information [43]. Its calculation formula is Equation (48):

$$H(m) = -\sum_{i=0}^{255} P(x_i) \times \log P(x_i) \quad (48)$$

where $H(m)$ represents the information entropy, m represents the information source, x_i represents the gray value of the pixel value i , and $P(x_i)$ represents the probability of the gray value.

The closer the information entropy is to eight, the stronger the randomness of the image and the higher the security performance of its encryption algorithm. We selected multiple sets of images from the USC-SIPI image database for testing, and Table 4 is a comparison of our results with other methods, bold indicates indicators of better performance. The results show that the entropy of the images encrypted by our method is closer to eight.

Table 4. Information entropy of encrypted images.

Images	Size	Plain Image	Cipher Image		
			Ref. [6]	Ref. [12]	Ours
5.1.09	256 * 256	6.7093	7.9973	7.9971	7.9970
5.1.10	256 * 256	7.3118	7.9973	7.9974	7.9977
5.1.11	256 * 256	6.4523	7.9970	7.9969	7.9974
5.1.12	256 * 256	6.7057	7.9975	7.9972	7.9974
5.1.13	256 * 256	1.5483	7.9972	7.9969	7.9974
5.1.14	256 * 256	7.3424	7.9970	7.9974	7.9977
5.2.08	512 * 512	7.5237	7.9992	7.9993	7.9994
5.2.09	512 * 512	6.9940	7.9994	7.9993	7.9993
5.2.10	512 * 512	5.7056	7.9993	7.9993	7.9993
5.3.01	1024 * 1024	7.5237	7.9998	7.9998	7.9998
5.3.02	1024 * 1024	6.8303	7.9998	7.9998	7.9997
7.1.01	512 * 512	6.0274	7.9993	7.9991	7.9993
7.1.02	512 * 512	4.0045	7.9993	7.9992	7.9994
7.1.03	512 * 512	5.4957	7.9993	7.9993	7.9994
7.1.04	512 * 512	6.1074	7.9992	7.9993	7.9993
7.1.05	512 * 512	6.5632	7.9993	7.9992	7.9993
7.1.06	512 * 512	6.6953	7.9992	7.9993	7.9993
7.1.07	512 * 512	5.9916	7.9993	7.9993	7.9992
7.1.08	512 * 512	5.0534	7.9994	7.9993	7.9992
7.1.09	512 * 512	6.1898	7.9993	7.9992	7.9994
7.1.10	512 * 512	5.9088	7.9993	7.9993	7.9993
7.2.01	1024 * 1024	5.6415	7.9998	7.9998	7.9998
boat.512	512 * 512	7.1914	7.9993	7.9994	7.9994
gray21.512	512 * 512	4.3923	7.9992	7.9994	7.9993
ruler.512	512 * 512	0.5000	7.9993	7.9992	7.9993
Mean of 256 * 256	256 * 256	-	7.9972	7.9972	7.9974
Mean of 512 * 512	512 * 512	-	7.9993	7.9993	7.9993
Mean of 1024 * 1024	1024 * 1024	-	7.9998	7.9998	7.9998

4.6. Antidifferential Attack (NPCR and UACI Standard Evaluation)

Differential attack is to change specific elements of the plaintext image, corresponding to the degree of influence of different ciphertexts, to obtain as much of the key as possible. The ability of an encryption algorithm to resist differential attacks can be measured by two important parameters: number of pixel change rate (NPCR) and uniform average change intensity (UACI) [44], which are calculated as Equation (49)–(51):

$$C(i, j) = \begin{cases} 0, & \text{if } T_1(i, j) = T_2(i, j) \\ 1, & \text{if } T_1(i, j) \neq T_2(i, j) \end{cases} \quad (49)$$

$$NPCR = \frac{\sum_{i=1}^m \sum_{j=1}^n C(i, j)}{m \times n} \times 100\% \quad (50)$$

$$UACI = \frac{\sum_{i=1}^m \sum_{j=1}^n |T_1(i, j) - T_2(i, j)|}{255 \times m \times n} \times 100\% \quad (51)$$

where m and n are the height and width of the image, and T_1 and T_2 represent the encrypted ciphertext images of two different original images.

In the paper [44], we can see the theoretical values of the three levels of NPCR and UACI for images of different sizes. We chose the confidence level to be 0.05 and tested the images in the USC-SIPI image database. The results are shown in Table 5, which shows that our results are in line with the theoretical expectations, underlined data indicates that the test did not pass, so our algorithm can resist differential attacks.

Table 5. NPCR and UACI for different images (%).

Image	NPCR				UACI				
	$\alpha = 0.05$	Ref. [6]	Ref. [7]	Ref. [8]	Proposed	Ref. [6]	Ref. [7]	Ref. [8]	Proposed
256 * 256	Theoretical NPCR	99.5693				Theoretical UACI	33.2824~33.6447		
5.1.09	99.6109	99.603	<u>99.5124</u>	99.5787	33.4475	33.552	33.5214	33.3580	
5.1.10	99.5972	99.636	99.6121	99.6565	33.4846	33.453	33.4215	33.5306	
5.1.11	99.5865	99.942	99.5943	99.5860	33.4482	33.586	33.4014	33.5725	
5.1.12	99.6323	99.792	99.5811	99.5992	33.4453	33.453	33.4158	33.5240	
5.1.13	99.6216	99.792	99.5963	99.5802	33.4531	33.520	33.4236	33.4265	
5.1.14	99.6078	99.621	99.5945	99.5831	33.4293	33.440	33.3951	33.5393	
512 * 512	Theoretical NPCR	99.5893				Theoretical UACI	33.3730~33.5541		
5.2.08	99.6105	99.960	<u>99.5878</u>	99.6136	33.5035	<u>33.692</u>	33.3978	33.5362	
5.2.09	99.6033	99.876	<u>99.5812</u>	99.6022	33.4674	33.548	33.4182	33.3835	
5.2.10	99.6101	99.654	<u>99.6100</u>	99.6147	33.4253	33.454	33.4263	33.4199	
7.1.01	99.6136	99.957	99.6028	99.6310	33.4885	<u>33.648</u>	33.4474	33.5258	
7.1.02	99.6040	99.918	99.6078	99.6151	33.4508	33.465	33.4326	33.4589	
7.1.03	99.6101	99.849	99.5811	99.6124	33.4352	<u>33.273</u>	33.4836	33.4771	
7.1.04	99.6178	99.991	99.5946	99.5930	33.5024	<u>33.202</u>	33.4782	33.4340	
7.1.05	99.5979	99.942	99.5937	99.6136	33.4739	<u>33.830</u>	33.4716	33.4699	
7.1.06	99.6269	99.670	99.5912	99.6041	33.4764	<u>33.627</u>	33.4365	33.4511	
7.1.07	99.6193	99.983	99.6014	99.5995	33.4310	<u>33.609</u>	33.4313	33.4637	
7.1.08	99.5979	99.818	99.6013	99.6170	33.4997	33.375	33.4460	33.4841	
7.1.09	99.6113	99.874	99.6148	99.6109	33.4630	33.530	33.3856	33.4925	
7.1.10	99.6166	99.697	99.6097	99.6079	33.4701	33.438	33.3941	33.4423	
boat.512	99.6227	99.715	99.6101	99.6212	33.4448	33.374	33.3973	33.4156	
gray21.512	99.6067	99.643	99.6034	99.5946	33.5113	33.507	33.4089	33.4367	
ruler.512	99.6124	99.637	99.5945	99.6056	33.4620	33.415	33.4635	33.4649	
1024 * 1024	Theoretical NPCR	99.5994				Theoretical UACI	33.4183~33.5088		
5.3.01	99.6067	99.950	99.6032	99.6294	33.5013	33.508	33.4392	33.5005	
5.3.02	99.6015	99.982	99.6108	99.6128	33.4255	<u>33.514</u>	33.4547	33.4263	
7.2.01	99.6005	99.980	99.6036	99.6088	33.4438	33.487	33.4301	33.4511	
Mean	99.6098	99.8192	99.5957	99.6076	33.4634	33.5	33.4329	33.4674	
Std	0.0103	0.2665	0.0200	0.0173	0.0268	0.0459	0.0328	0.0518	
Pass/All	25/25	25/25	22/25	25/25	25/25	17/25	25/25	25/25	

4.7. Anticlipping and Noise Attacks

When the image information is transmitted on the channel, the image information may be subjected to cropping attacks, noise attacks, and other attack methods by the attacker so that the transmitted image information is damaged, and the useful information cannot be obtained after decryption with the correct key. Therefore, we conducted cropping attack and noise attack tests on the images respectively to check the robustness of our algorithm. We used the peak signal-to-noise ratio (PSNR) between the ciphertext image and the plaintext image as a standard [45], and its calculation formula is as Equations (52) and (53):

$$MSE = \frac{\sum_{i=1}^m \sum_{j=1}^n (T_1(i, j) - T_2(i, j))^2}{m \times n} \quad (52)$$

$$PSNR = 20 * \log_{10} \left(\frac{255}{\sqrt{MSE}} \right) \quad (53)$$

where $m \times n$ is the image size, and $T_1(i, j)$ and $T_2(i, j)$ represent the original image and the encrypted image.

We cropped the image by 1/16, 1/8, 1/4, and 1/2, and set the pixel value of these parts to zero. Table 6 shows the peak signal-to-noise ratio (PSNR) of different degrees of cropping attack; Figure 17 shows the decrypted image after the ciphertext is subjected to different degrees of cropping attack. We can see that the general information of the decrypted image

can still be identified after being subjected to different degrees of cropping attack; therefore, our algorithm is resistant to clipping attacks.

Table 6. PSNR of different degrees of clipping attack.

Area	1/16	1/8	1/4	1/2
PSNR	21.314192	18.380856	15.342343	12.250188

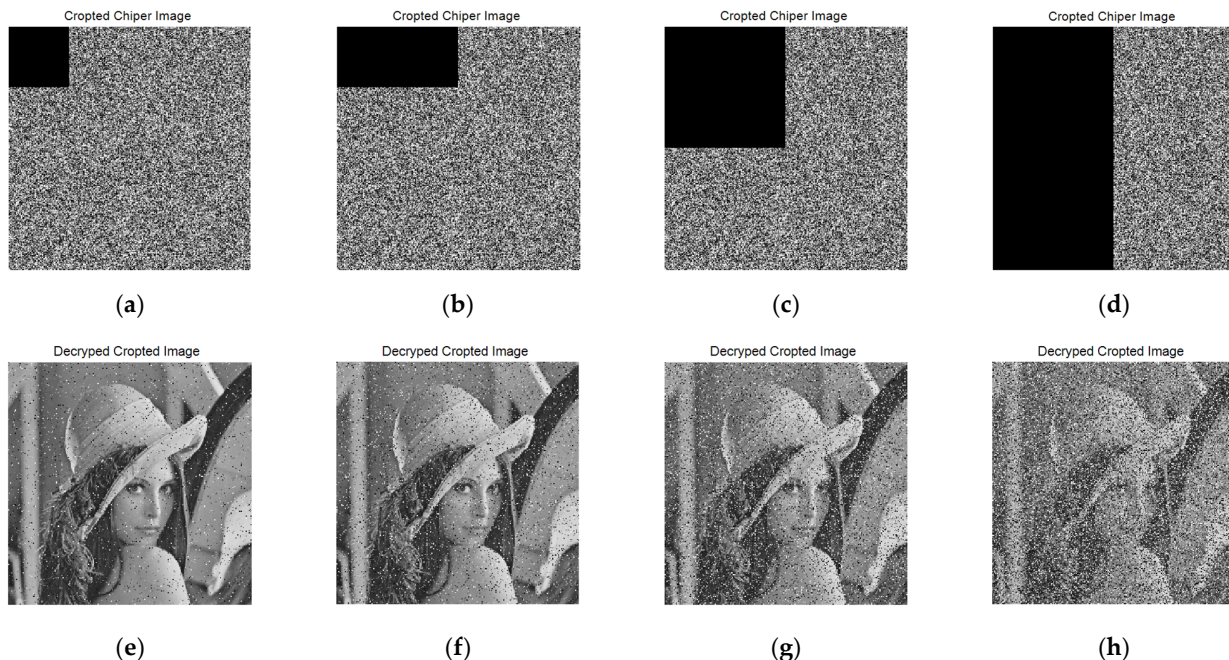


Figure 17. Decrypted images for varying degrees of cropping attacks: (a) 1/16 crop; (b) 1/8 crop; (c) 1/4 crop; (d) 1/2 crop; (e–h) decrypted images of (a–d).

Then, we applied noise of 0.01, 0.05, and 0.15 intensity to the ciphertext image and decrypted it with the correct key. The PSNR of the decrypted image is shown in Table 7, and the decrypted image is shown in Figure 18, which means that our algorithm is also resistant to noise attacks.

Table 7. PSNR for noise attack.

Noise Level	0.01 Level	0.05 Level	0.1 Level
PSNR	28.971428	22.408105	19.258843

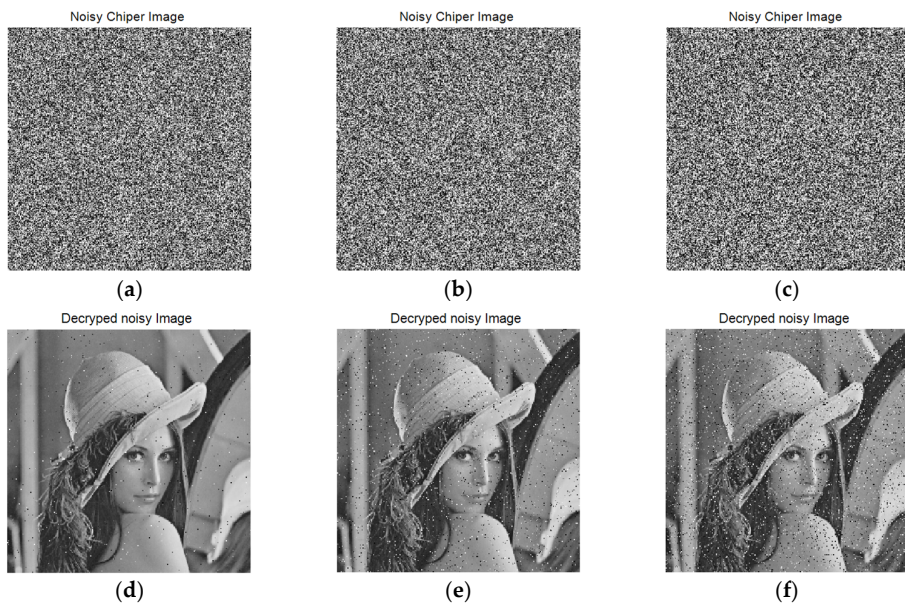


Figure 18. Noise attack test results: (a–c) noisy cipher image of different noise level; (d–f) decrypted noisy image.

4.8. Key Space Analysis

When the key space is large enough, the algorithm can resist brute force attack. The key in this paper has four parts: initial parameters $d_1 \sim d_8$, $sumP$ of plaintext image pixel values, image block size $Bsize$, supplementary parameters $M1$, $N1$, and the number of blocks $Bnum$. The calculation accuracy is 10^{-15} . Taking a $256 * 256$ image as an example, the main key space is Equation (54):

$$keyspace = 10^{15} * 8 + 10^8 + 10 + 20 + 10^2 > 2^{100} \quad (54)$$

Its key space is much larger than 2^{100} , so it can resist brute force attacks [46].

4.9. Key Sensitivity Analysis

An encryption algorithm is sufficiently secure when it is sensitive to subtle changes in the key, so we tested this on the peppers images. Since our main initial keys $d_1 \sim d_8$ are generated by the SHA-512 function, we randomly selected the correct key key , then increased the last digit sequence value generated by SHA-512 by 1, and then calculated and generated a new initial key $key1$, which was only slightly different from the correct key. Figure 19 shows the results of decryption with the changed key, indicating that our method has better key sensitivity.

$key\ hash\ value = (275afc80927870608dfa79743a56d02e3ff7d009aa78655e9affbcb25e74e1ce102df926ffe0670ca599cc5ef2d57299429bfba3d45b66143fb075b69e590896);$

$key = (0.385365853658537, 0.412682926829268, 0.578536585365854, 0.237354085603113, 0.038910505836576, 0.578947368421053, 0.578947368421053, 0.290448343079922);$

$key1\ hash\ value = (275afc80927870608dfa79743a56d02e3ff7d009aa78655e9affbcb25e74e1ce102df926ffe0670ca599cc5ef2d57299429bfba3d45b66143fb075b69e590897);$

$key1 = (0.385365853658537, 0.412682926829268, 0.578536585365854, 0.237354085603113, 0.038910505836576, 0.578947368421053, 0.426900584795322, 0.391812865497076);$

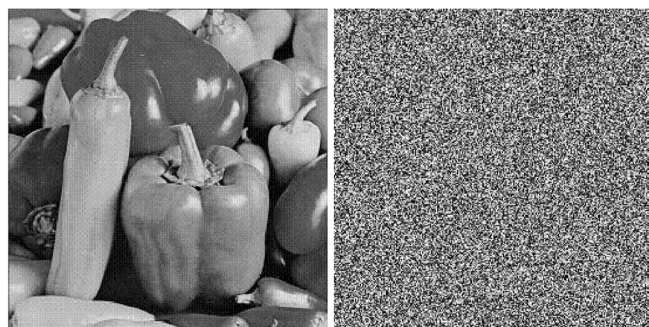


Figure 19. Decryption result of correct key *key* and changed key *key1*.

4.10. Computational Complexity

Our computational complexity is divided into three parts: generation of initial values, disorder, and diffusion. In the process of generating initial values, we computed them within a constant value $O(m * n)$, where m and n denote images and rows and columns, respectively. In the process of dislocation, we dislocated between B_{num} layers and B_{size} layers, and its computational complexity is a constant value $O(b)$, where b denotes the corresponding maturity. In the process of diffusion, we performed cubic diffusion, whose computational complexity $O(x * y * z)$, x, y, z are the sizes of the three dimensions of the probability amplitude matrix. With the change of image size and resolution, its computational complexity is $O(m * n) + O(x * y * z)$, which is roughly the same for different images. Therefore, it can be better implemented in practical applications.

5. Conclusions

In this paper, we propose a 3D cuboid image encryption scheme based on message-encoded controlled alternate quantum walks. We used SHA-512 to obtain the key set and used the key set to generate the system parameters of a one-dimensional discrete quantum walk and controlled alternate quantum walk on a circle. Then, we used the one-dimensional discrete quantum walk model and controlled alternating quantum walk model encrypted image to design a three-dimensional cuboid image encryption algorithm. In the scrambling stage, the image was scrambled between layers and layer-by-layer cross-sections; in the diffusion stage, the pixel binary cube was rotated first and combined with the 3D quantum hash, then XORed with the 3D quantum hash sequence and tiled to obtain the encrypted image. Simulation results and image data tests show that the scheme can resist various typical attacks and has good security performance. In the future, we plan to introduce advanced, new technologies and methods [47–52], such as deep learning models, neural networks, some concepts of image fusion and recognition, etc. into image encryption and further propose new algorithms with better encryption effects.

Author Contributions: Data curation, P.L.; Formal analysis, P.L.; Investigation, P.L.; Methodology, S.Z.; Project administration, S.Z.; Software, W.Q.Y.; Supervision, W.Q.Y.; Validation, P.L.; Writing—original draft, P.L.; Writing—review and editing, S.Z. All authors have read and agreed to the published version of the manuscript.

Funding: This work is supported by the National Key Technology R&D Program of China (No. 2018YFC0910500), the National Natural Science Foundation of China (Nos. 62272079, 61751203, 61972266, 61802040), Liaoning Revitalization Talents Program (No. XLYC2008017), the Innovation and Entrepreneurship Team of Dalian University (No. XQN202008), Natural Science Foundation of Liaoning Province (Nos. 2021-MS-344, 2021-KF-11-03, 2022-KF-12-14).

Data Availability Statement: Not applicable.

Conflicts of Interest: The authors declare no conflict of interest.

References

- Wan, W.; Wang, J.; Li, J.; Sun, J.; Zhang, H.; Liu, J. Hybrid JND model-guided watermarking method for screen content images. *Multimed. Tools Appl.* **2020**, *79*, 4907–4930. [[CrossRef](#)]
- Aminuddin, A.; Ernawan, F. AuSR2: Image watermarking technique for authentication and self-recovery with image texture preservation. *Comput. Electr. Eng.* **2022**, *102*, 108207. [[CrossRef](#)]
- Cao, W.; Mao, Y.; Zhou, Y. Designing a 2D infinite collapse map for image encryption. *Signal Process.* **2020**, *171*, 107457. [[CrossRef](#)]
- Man, Z.; Li, J.; Di, X.; Sheng, Y.; Liu, Z. Double image encryption algorithm based on neural network and chaos. *Chaos Solitons Fractals* **2021**, *152*, 111318. [[CrossRef](#)]
- Singh, K.N.; Singh, A.K. Towards integrating image encryption with compression: A survey. *ACM Trans. Multimed. Comput. Commun. Appl.* **2022**, *18*, 1–21. [[CrossRef](#)]
- Yan, X.; Liu, F.; Yan, W.Q.; Yang, G.; Lu, Y. Weighted visual cryptographic scheme with improved image quality. *Multimed. Tools Appl.* **2020**, *79*, 21345–21360. [[CrossRef](#)]
- Wang, T.; Wang, M.-H. Hyperchaotic image encryption algorithm based on bit-level permutation and DNA encoding. *Opt. Laser Technol.* **2020**, *132*, 106355. [[CrossRef](#)]
- Khalil, N.; Sarhan, A.; Alshewimy, M.A. An efficient color/grayscale image encryption scheme based on hybrid chaotic maps. *Opt. Laser Technol.* **2021**, *143*, 107326. [[CrossRef](#)]
- Zhou, S. A real-time one-time pad DNA-chaos image encryption algorithm based on multiple keys. *Opt. Laser Technol.* **2021**, *143*, 107359. [[CrossRef](#)]
- Zhang, Y. The fast image encryption algorithm based on lifting scheme and chaos. *Inf. Sci.* **2020**, *520*, 177–194. [[CrossRef](#)]
- Wang, X.; Guan, N.; Yang, J. Image encryption algorithm with random scrambling based on one-dimensional logistic self-embedding chaotic map. *Chaos Solitons Fractals* **2021**, *150*, 111117. [[CrossRef](#)]
- Alawida, M.; Teh, J.S.; Samsudin, A. An image encryption scheme based on hybridizing digital chaos and finite state machine. *Signal Process.* **2019**, *164*, 249–266. [[CrossRef](#)]
- Himeur, Y.; Boukabou, A. A robust and secure key-frames based video watermarking system using chaotic encryption. *Multimed. Tools Appl.* **2018**, *77*, 8603–8627. [[CrossRef](#)]
- Yu, J.; Xie, W.; Zhong, Z.; Wang, H. Image encryption algorithm based on hyperchaotic system and a new DNA sequence operation. *Chaos Solitons Fractals* **2022**, *162*, 112456. [[CrossRef](#)]
- Jasra, B.; Moon, A.H. Color image encryption and authentication using dynamic DNA encoding and hyper chaotic system. *Expert Syst. Appl.* **2022**, *206*, 117861. [[CrossRef](#)]
- Qiu, H.; Xu, X.; Jiang, Z.; Sun, K.; Xiao, C. A color image encryption algorithm based on hyperchaotic map and Rubik’s Cube scrambling. *Nonlinear Dyn.* **2022**, *1*–19. [[CrossRef](#)]
- Mansouri, A.; Wang, X. A novel one-dimensional chaotic map generator and its application in a new index representation-based image encryption scheme. *Inf. Sci.* **2021**, *563*, 91–110. [[CrossRef](#)]
- Wang, X.; Zhao, M. An image encryption algorithm based on hyperchaotic system and DNA coding. *Opt. Laser Technol.* **2021**, *143*, 107316. [[CrossRef](#)]
- Xian, Y.; Wang, X. Fractal sorting matrix and its application on chaotic image encryption. *Inf. Sci.* **2021**, *547*, 1154–1169. [[CrossRef](#)]
- Jithin, K.; Sankar, S. Colour image encryption algorithm combining Arnold map, DNA sequence operation, and a Mandelbrot set. *J. Inf. Secur. Appl.* **2020**, *50*, 102428. [[CrossRef](#)]
- Gao, W.; Sun, J.; Qiao, W.; Zhang, X. Digital image encryption scheme based on generalized Mandelbrot-Julia set. *Optik* **2019**, *185*, 917–929. [[CrossRef](#)]
- Gao, Y.; Jiao, S.; Fang, J.; Lei, T.; Xie, Z.; Yuan, X. Multiple-image encryption and hiding with an optical diffractive neural network. *Opt. Commun.* **2020**, *463*, 125476. [[CrossRef](#)]
- Chen, H.; Liu, Z.; Tanougast, C.; Liu, F. A novel chaos based optical cryptosystem for multiple images using DNA-blend and gyrator transform. *Opt. Lasers Eng.* **2021**, *138*, 106448. [[CrossRef](#)]
- Wang, F.; Ni, R.; Wang, J.; Zhu, Z.; Hu, Y. Invertible encryption network for optical image cryptosystem. *Opt. Lasers Eng.* **2022**, *149*, 106784. [[CrossRef](#)]
- Zhang, Y.; Chen, A.; Tang, Y.; Dang, J.; Wang, G. Plaintext-related image encryption algorithm based on perceptron-like network. *Inf. Sci.* **2020**, *526*, 180–202. [[CrossRef](#)]
- Ding, Y.; Wu, G.; Chen, D.; Zhang, N.; Gong, L.; Cao, M.; Qin, Z. DeepEDN: A deep-learning-based image encryption and decryption network for internet of medical things. *IEEE Internet Things J.* **2020**, *8*, 1504–1518. [[CrossRef](#)]
- Yu, F.; Zhang, Z.; Shen, H.; Huang, Y.; Cai, S.; Du, S. FPGA implementation and image encryption application of a new PRNG based on a memristive Hopfield neural network with a special activation gradient. *Chin. Phys. B* **2022**, *31*, 020505. [[CrossRef](#)]
- Shi, Y.; Hu, Y.; Wang, B. Image encryption scheme based on multiscale block compressed sensing and Markov model. *Entropy* **2021**, *23*, 1297. [[CrossRef](#)]
- Sun, C.; Wang, E.; Zhao, B. Image encryption scheme with compressed sensing based on a new six-dimensional non-degenerate discrete hyperchaotic system and plaintext-related scrambling. *Entropy* **2021**, *23*, 291. [[CrossRef](#)]
- Wang, X.; Li, Y. Chaotic image encryption algorithm based on hybrid multi-objective particle swarm optimization and DNA sequence. *Opt. Lasers Eng.* **2021**, *137*, 106393. [[CrossRef](#)]

31. Abbasi, A.A.; Mazinani, M.; Hosseini, R. Chaotic evolutionary-based image encryption using RNA codons and amino acid truth table. *Opt. Laser Technol.* **2020**, *132*, 106465. [[CrossRef](#)]
32. Liang, Z.; Qin, Q.; Zhou, C. An image encryption algorithm based on Fibonacci Q-matrix and genetic algorithm. *Neural Comput. Appl.* **2022**, *34*, 19313–19341. [[CrossRef](#)]
33. Liu, X.; Xiao, D.; Huang, W.; Liu, C. Quantum block image encryption based on arnold transform and sine chaotification model. *IEEE Access* **2019**, *7*, 57188–57199. [[CrossRef](#)]
34. Wang, J.; Chen, J.; Wang, F.; Ni, R. Optical image encryption scheme based on quantum s-box and meaningful ciphertext generation algorithm. *Opt. Commun.* **2022**, *525*, 128834. [[CrossRef](#)]
35. Ma, Y.; Li, N.; Zhang, W.; Wang, S.; Ma, H. Image encryption scheme based on alternate quantum walks and discrete cosine transform. *Opt. Express* **2021**, *29*, 28338–28351. [[CrossRef](#)] [[PubMed](#)]
36. Khan, M.; Hussain, I.; Jamal, S.S.; Amin, M. A privacy scheme for digital images based on quantum particles. *Int. J. Theor. Phys.* **2019**, *58*, 4293–4310. [[CrossRef](#)]
37. Yan, T.; Li, D. A Novel Quantum Color Image Encryption Scheme Based on Controlled Alternate Quantum Walks. In Proceedings of the International Conference on Security, Privacy and Anonymity in Computation, Communication and Storage, New York, NY, USA, 9–13 August 2021; Springer: Cham, Switzerland, 2021; pp. 519–530.
38. Yang, Y.-G.; Pan, Q.-X.; Sun, S.-J.; Xu, P. Novel image encryption based on quantum walks. *Sci. Rep.* **2015**, *5*, 7784. [[CrossRef](#)] [[PubMed](#)]
39. Yang, Y.-G.; Xu, P.; Yang, R.; Zhou, Y.-H.; Shi, W.-M. Quantum Hash function and its application to privacy amplification in quantum key distribution, pseudo-random number generation and image encryption. *Sci. Rep.* **2016**, *6*, 19788. [[CrossRef](#)] [[PubMed](#)]
40. Abd EL-Latif, A.A.; Abd-El-Atty, B.; Abou-Nassar, E.M.; Venegas-Andraca, S.E. Controlled alternate quantum walks based privacy preserving healthcare images in internet of things. *Opt. Laser Technol.* **2020**, *124*, 105942. [[CrossRef](#)]
41. Abd EL-Latif, A.A.; Abd-El-Atty, B.; Venegas-Andraca, S.E. Controlled alternate quantum walk-based pseudo-random number generator and its application to quantum color image encryption. *Phys. A Stat. Mech. Appl.* **2020**, *547*, 123869. [[CrossRef](#)]
42. Boriga, R.E.; Dăscălescu, A.C.; Diaconu, A.V. A new fast image encryption scheme based on 2D chaotic maps. *IAENG Int. J. Comput. Sci.* **2014**, *41*, 249–258.
43. Shannon, C.E. A mathematical theory of communication. *Bell Syst. Tech. J.* **1948**, *27*, 379–423. [[CrossRef](#)]
44. Wu, Y.; Noonan, J.P.; Agaian, S. NPCR and UACI randomness tests for image encryption. *Cyber J. Multidiscip. J. Sci. Technol. J. Sel. Areas Telecommun.* **2011**, *1*, 31–38.
45. Hore, A.; Ziou, D. Image Quality Metrics: PSNR vs. SSIM. In Proceedings of the 2010 20th International Conference on Pattern Recognition, Istanbul, Turkey, 23–26 August 2010; pp. 2366–2369.
46. Alvarez, G.; Li, S. Some basic cryptographic requirements for chaos-based cryptosystems. *Int. J. Bifurc. Chaos* **2006**, *16*, 2129–2151. [[CrossRef](#)]
47. Li, Y. Research and Application of Deep Learning in Image Recognition. In Proceedings of the 2022 IEEE 2nd International Conference on Power, Electronics and Computer Applications (ICPECA), Shenyang, China, 21–23 January 2022; pp. 994–999.
48. Falsettta, A.; Roveri, M. Privacy-preserving deep learning with homomorphic encryption: An introduction. *IEEE Comput. Intell. Mag.* **2022**, *17*, 14–25. [[CrossRef](#)]
49. Chen, J.; Qiu, X.; Ding, C.; Wu, Y. SAR image classification based on spiking neural network through spike-time dependent plasticity and gradient descent. *ISPRS J. Photogramm. Remote Sens.* **2022**, *188*, 109–124. [[CrossRef](#)]
50. Yan, S.; Gu, Z.; Park, J.H.; Xie, X. Synchronization of delayed fuzzy neural networks with probabilistic communication delay and its application to image encryption. *IEEE Trans. Fuzzy Syst.* **2022**. [[CrossRef](#)]
51. Li, J.; Liu, J.; Zhou, S.; Zhang, Q.; Kasabov, N.K. Learning a coordinated network for detail-refinement multi-exposure image fusion. *IEEE Trans. Circuits Syst. Video Technol.* **2022**. [[CrossRef](#)]
52. Feng, L.; Chen, X. Image recognition and encryption algorithm based on artificial neural network and multidimensional chaotic sequence. *Comput. Intell. Neurosci.* **2022**, *2022*, 9576184. [[CrossRef](#)]